# Solution-Processable 2D Materials Applied in Light-Emitting Diodes and Solar Cells

*Antonio Gaetano Ricciardulli and Paul W. M. Blom\**

The last decades have witnessed a remarkable scientific progress in the field of organic and perovskite optoelectronics. Two-dimensional (2D) materials are an attractive building block for next-generation devices, thanks to their unique physical, optical, and electric characteristics including atomically thin bodies, high transmittance, ultralight weight, and tunable band structures. The state-of-the-art optoelectronic devices utilizing 2D materials mainly rely on 2D thin films grown by chemical vapor deposition. Although good device performances have been demonstrated, a huge gap between fundamental studies and practical applications remains, because of the high cost and troublesome transfer/restacking processes. Therefore, flexible and transparent light-emitting diodes (LEDs) and solar cells (SCs) containing solution-processed 2D materials from top-down exfoliation methods have recently emerged as promising candidates for future light conversion and emission devices. They combine ease of processing, tailorable optoelectronic features, facile integration with complementary layers, compatibility with arbitrary substrates, and enhanced performances. In addition, the latest processing techniques (such as ink-jet printing, spray coating) also offer the opportunity for the scaled-up fabrication of square-meter-scale low-cost device systems. Recent advances, challenges, and future perspectives of solution-processed 2D materials for usage in emerging LEDs and SCs applications are discussed here.

## 1. Introduction

Two-dimensional (2D) materials have been successfully exploited in a wide range of applications including catalysts,[1] batteries,[2] supercapacitors,[3] and sensors[4] because of their unprecedented chemical and physical properties. Recently, 2D materials have also emerged as potential candidates for optoelectronic devices,[5] since their tunable optical and electronic properties,[6] light

weight,[7] and flexibility[8] can serve a diverse range of functions. In this frame, the 2D family offers a broad and versatile supply to meet the requirements of solar cells (SCs) and light-emitting diodes (LEDs), which are assembled into stacked structures of different components with specific functionalities. As proof of concept, materials like graphene and its derivatives, transition metals dichalcogenides (TMDCs) and black phosphorus (BP) have been successfully embedded into organic SCs (OSCs) and perovskite SCs (PeSCs) and LEDs in the last years.[9] However, their practical use is hindered by high cost and complex synthetic methodologies. To integrate 2D materials into emerging solution-processed optoelectronic devices, which rely on low cost to be competitive in the market, high quality should be coupled with cost effectiveness. Hence, further efforts have been recently made in terms of materials synthesis to turn laboratory-scale research into commercial applications.[10] Solution-processed approaches meet this direction through ease of processing, cost effectiveness, and structure/properties tailoring.

This article presents the recent breakthrough advances in the fabrication and engineering of solution-processable 2D materials, such as high-quality graphene, functionalized graphene materials, BP, and TMDCs, for light-emitting and harvesting applications. The review will provide a perspective in future integration of 2D materials into optoelectronics, in particular LEDs and SCs, based on the comprehensive analysis of their up-to-date progress, spanning from the synthetic routes to the processing techniques. The report starts with an overview on optical and electric properties of 2D materials, followed by the development of their synthesis and processing strategies. Subsequently, their applicability in emerging LEDs and SCs is demonstrated, followed by a discussion on the challenges and possible opportunities to further eliminate the practical limitations of current optoelectronic devices.

## 2. Fundamentals of 2D Materials for Optoelectronics

The realm of the 2D materials lends an immense selection of optical, electric, and physical functionalities that can be utilized in novel LEDs and SCs. In this section, the fundamental properties of 2D materials are briefly discussed.

Dr. A. G. Ricciardulli, Prof. P. W. M. Blom
Max Planck Institute for Polymer Research
Ackermannweg 10, 55128 Mainz, Germany
E-mail: blom@mpip-mainz.mpg.de
Dr. A. G. Ricciardulli
Department of Materials Science
Technische Universität Darmstadt
Alarich-Weiss-Straße 2, 64287 Darmstadt, Germany

## 2.1. High-Quality Graphene and Functionalized Derivatives

Graphene is a monolayer of graphite (**Figure 1**a),[11] endowed with outstanding properties, which made it one of the most investigated materials of the last decades. The carbon atoms in graphene are arranged in a honeycomb lattice and characterized by sp²-hybridization, which results in three localized $\sigma$ bonds on the planar assembly and a delocalized conjugated $\pi$ bond in the perpendicular direction. This structure, in case of an ideal single-layer graphene, has a zero-gap semi-metal character (Figure 1b), due to its valence and the conduction bands (VB and CB, respectively) that touch at the K(K′) points of the Brillouin zone.[12] As a consequence, graphene can absorb a broad light spectrum, spanning from the ultraviolet to infrared region.[13] It is worth mentioning that the bandgap of graphene can be opened in the low-energy regime by tailoring its electronic structure, which broadens the range of application for graphene. For this purpose, there are different methods, such as the introduction of defects,[14] chemical doping,[15] post-functionalization,[16] and size-confinement.[17] Reported intrinsic carrier mobility of single-layer graphene reaches values up to 20 000 $cm^{-2}$ $V^{-1}$ $s^{-1}$.[18] Furthermore, as one of the most important features for optoelectronic devices, a monolayer of graphene shows an optical transmittance of 97.7%.[19] However, despite these outstanding features, a single layer of this carbon allotrope is limited by a sheet resistance (Rs) of ≈6 kΩ $sq^{-1}$.[20] To increase the solubility and processability, graphene has been functionalized with oxygen-containing groups.[21] Graphene oxide (GO) and reduced GO (rGO) have been widely used in optoelectronics because of their versatility.[22] However, the disruption of the aromaticity from the functional groups leads to a general decrease of the optical and electric properties.[23] In addition to the remarkable optical and electronic properties, graphene and its functional derivatives, like other 2D materials, have the enormous advantage to be extremely thin and flexible.[24] These features are becoming increasingly relevant in optoelectronics, where the latest trend is the fabrication of ultrathin and flexible devices.

**Antonio Gaetano Ricciardulli** received his Ph.D. degree in chemistry in 2018 at the Max Planck Institute for Polymer Research (MPI-P), Mainz, Germany, working on solution-processed 2D materials for optoelectronics. After a post-doc experience at MPI-P in the field of perovskite light-emitting diodes, he joined the TU-Darmstadt as a postdoctoral scientist. His current research interests focus on perovskite optoelectronics and 2D materials applications.

**Paul W. M. Blom**, received his Ph.D. degree in 1992 from the Technical University Eindhoven, Eindhoven, Netherlands, on picosecond charge carrier dynamics in GaAs. At Philips Research Laboratories, he was engaged in the electro-optical properties of polymer light-emitting diodes. From 2000, he held a professorship at the University of Groningen in the field of electrical and optical properties of organic semiconducting devices. In September 2008, he became a scientific director of the Holst Centre in Eindhoven, where the focus is on foil-based electronics, followed by an appointment as director at the MPI for polymer research in the field of molecular electronics in 2012.

## 2.2. Black Phosphorus

BP, also named as phosphorene, is the most thermodynamically stable phosphorus allotrope, which can be exfoliated into thin layers.[25] The crystal structure of an individual layer of BP is composed by units of four sp³-hybridized phosphorus atoms, resulting in a non-planar folded honeycomb structure (Figure 1c).[26] The sp³-hybridization generates two different bond lengths, 2.224 and 2.244 Å, which are in- and out-plane, respectively. Because of the puckered structure, BP shows highly anisotropic properties.[27] Indeed, phosphorene exhibits dichroism[28] and a huge variation of the optical absorption properties with direction.[29] BP displays anisotropic behavior also in carrier masses, which strictly relates to charge carrier mobility.[30] For instance, the calculated hole mobility along the zigzag direction, on the order of $10^4$ $cm^2$ $V^{-1}$ $s^{-1}$, is 40 times higher than the one in the armchair direction.[31] In addition to the above-mentioned properties, one of the most intriguing features of phosphorene for optoelectronic applications is the thickness-depended direct bandgap. A monolayer of BP has a predicted direct bandgap of ≈2 eV at the Γ point of the first Brillouin zone.[32] By adding other layers, the interlayer interactions lead to the reduction of the bandgap (Figure 1d) till the value of ≈0.3 eV (bulk BP).[33] This peculiar characteristic opens up novel possibilities for the integration of tailored 2D semiconductors in LEDs and SCs.

## 2.3. Transition Metal Dichalcogenides

TMDCs are a class of materials with the chemical formula $MX_2$, where M, a transition metal element (molybdenum [Mo], tungsten [W]) and X, a chalcogen element (sulfur [S], selenium [Se], or tellurium [Te]) are covalently bonded.[34] Depending on the specific chemical compositions, they can exist in different structural phases. The two most common phases (Figure 1e) are the octahedral (1T) and trigonal prismatic (2H) ones.[35] With regard to $MoS_2$ the first has the Mo atoms octahedrally coordinated with the S and Mo atoms, the latter has each Mo
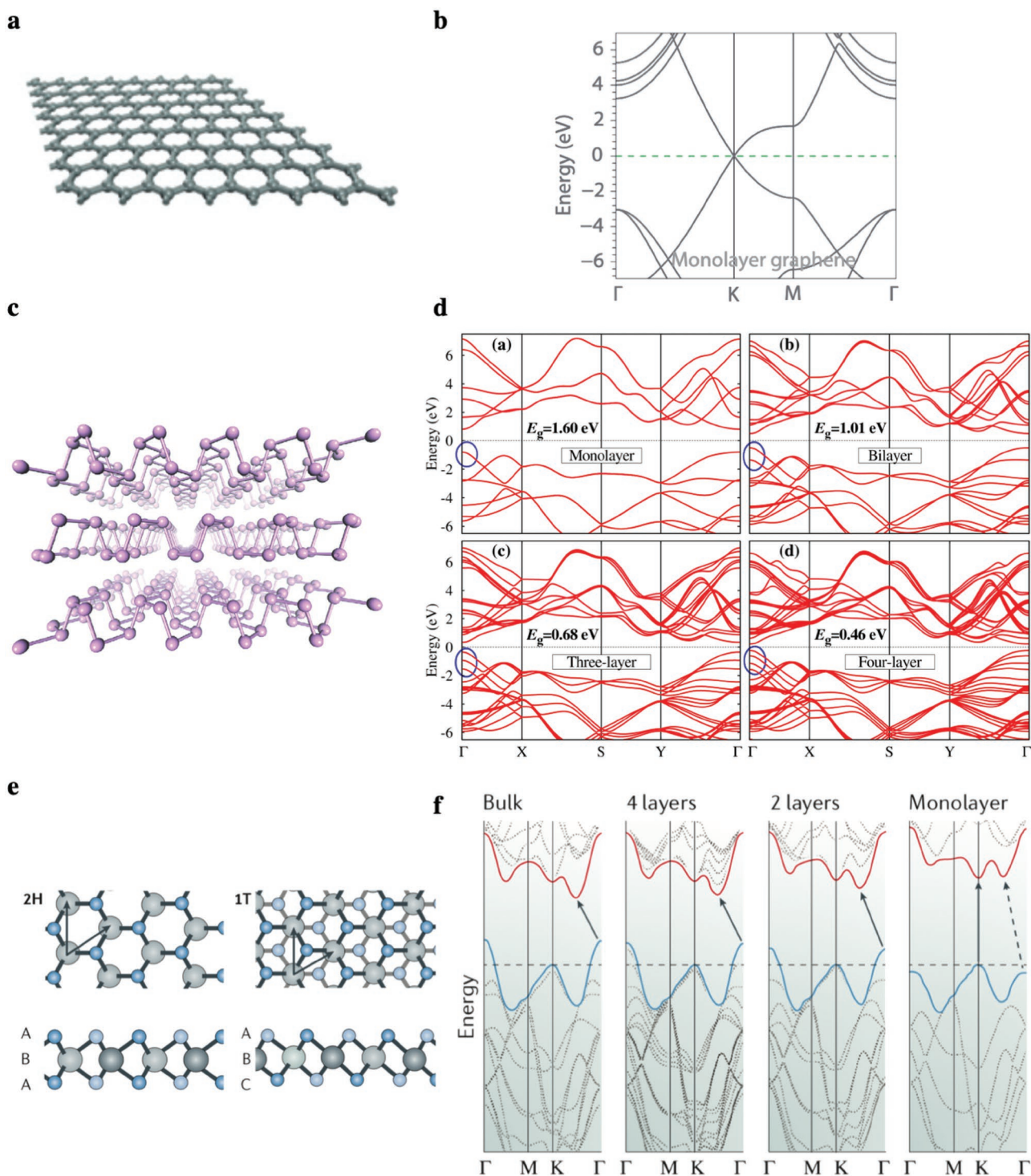
**Figure 1.** a) Atomic structure of a graphene monolayer and b) the related band structure. Reproduced with permission.[11b] Copyright 2014, Springer Nature. c) Atomic structure of BP. Reproduced with permission.[26] Copyright 2014, Springer Nature. d) Band structures for n-layered BP calculated within the GW approach for n between 1 and 4, blue circles show the band splitting near the gap. Reproduced with permission. [33] Copyright 2014, American Physical Society. e) Atomic structure of single layers of TMDCs in their 2H and 1T forms. Transition metal and chalcogen are illustrated in gray and blue spheres, respectively. f) Evolution of the band structure of 2H-$MoS_2$ calculated for samples with different thickness. e,f) Reproduced with permission.[35] Copyright 2017, Springer Nature.

atom prismatically packed by six S atoms. As a result of the chemical and structural diversity, TMDCs exhibit a wide assortment of electronic properties. Materials such as $MoS_2$ and $WS_2$ present semiconducting behavior in their thermodynamically stable 2H phases, which makes them attracting for electronic applications.[36] Furthermore, they have thickness-dependent

**ADVANCED
SCIENCE NEWS**
www.advancedsciencenews.com

**ADVANCED
MATERIALS
TECHNOLOGIES**
www.advmattechnol.de

electronic band structures (Figure 1f), showing an interlayer coupling effect.[37] Indeed, the indirect bandgap of bulk and few-layered 2H-MoS$_2$ turns into a direct bandgap for the monolayer. The indirect bandgap of the semiconductor 2H-MoS$_2$ (1.2 eV) gradually increases by reducing the thickness, up to ≈2.1 eV, in the case of the direct bandgap of a monolayer.[38] The indirect to direct bandgap transition from layered to single-layer TMDCs is further demonstrated by photoluminescence (PL) studies.[39] While PL of bulk MoS$_2$ and WS$_2$ is negligible, it emerges when the TMDCs are thinned into monolayers. Theoretical calculations for monolayer MoS$_2$ estimate an electron mobility of 10–1000 cm$^2$ V$^{-1}$ s$^{-1}$ at room temperature.[40] However, as for BP, practical experiments have determined much lower charge carrier mobility due to the presence of defects in these atomically thin layers.[41]

## 3. Synthesis and Processing of Solution-Processable 2D Materials

### 3.1. Scalable Synthetic Methods of 2D Materials

The structure of 2D materials has a strong impact on the properties of 2D materials. Hence, to guarantee high quality and to minimize the structural disorder, the choice of the synthetic route plays an essential role. Chemical vapor deposition (CVD) has been widely used for the production of high-quality 2D materials for optoelectronic applications.[42] Despite various efforts successfully proving the suitability of CVD-2D materials in devices such as SCs and LEDs, the complicated process, low yield, and high cost hinder their practical use.[43] Conversely, solution-processable approaches can be a valid alternative to synthesize 2D materials for application in optoelectronic devices, which, in addition to versatility and high performance, rely on low cost to hit the consumer market. The prominent methods are discussed in this section.

#### 3.1.1. Liquid-Phase Sonication

Liquid-phase sonication is a top-down method for the exfoliation of a variety of materials, such as graphite,[44] BP,[45] and TMDCs.[46] Liquid-phase sonication involves three major steps (**Figure 2**a):[47] 1) preparation and dispersion of bulk layered crystals into specific liquid media; 2) exfoliation of the dispersion through bath or tip sonication; and 3) purification of the resultant nanosheets by discarding unexfoliated material via density gradient centrifugation. The exfoliation of bulk material in thin layers is triggered by the collapse of bubbles, generated by ultrasonic cavitation, which results in normal and shear forces.[48]

Originally designed for the exfoliation of carbon nanotubes, Coleman first reported the effective exfoliation of graphite in a range of solvents.[49] Powdered graphite was immersed into different solvents and exposed to ultrasonication. To successfully exfoliate the graphite into graphene and avoid re-aggregation, it was found that the surface energies of the solvent and graphene (≈68 mJ m$^{-2}$) should be similar. The matching of their surface

energies results in a minimization of the mixing enthalpy, as suggested by the following equation[50]

$$\frac{\Delta H_{\text{mix}}}{V} \approx \frac{2}{T_{\text{NS}}}\left(\sqrt{E_{\text{s}}} - \sqrt{E_{\text{G}}}\right)^2 \varnothing_{\text{G}} \tag{1}$$

where $\frac{\Delta H_{\text{mix}}}{V}$ is the enthalpy of mixing for graphene flakes, $T_{\text{NS}}$ is the flake thickness, $E_{\text{S}}$ and $E_{\text{G}}$ are the solvent and the graphene surface energy, respectively, and $\varnothing_{\text{G}}$ is the dispersed graphene volume fraction.

**Table 1** shows the most commonly used solvents in graphite exfoliation with the related surface tensions. N-Methyl-2-pyrrolidone (NMP) is one the most efficient solvents to carry out the delamination of graphite through the sonication approach. Furthermore, NMP is an efficient solvent to exfoliate bulk BP, which provides stable and highly concentrated (≈0.4 mg mL$^{-1}$) 2D BP dispersions.[51] However, the high boiling point of the solvents generally used is problematic for practical applications. Binary mixtures of solvents with lower boiling points, such as t-butyl alcohol and isopropanol (IPA) in water,[52] or surfactants[53] can be used to enhance both exfoliation yield of graphite and MoS$_2$. Other methods require the use of longer sonication time.[54] However, the prolonged sonication causes defects in the exfoliated flakes, resulting in a sensible decrease of the electric and electronic properties. Liquid-phase sonication is a simple solution-processable route to exfoliate 2D crystals under ambient conditions without involving chemical reactions. Despite the mass-production potential, the large-scale application of sonication is hindered because of the low exfoliation efficiency, the wide thickness distribution, and the small fraction of large flakes. Recently, liquid-phase exfoliation technologies, such as high-shear mixing and micro-fluidization based on high-shear mixer-driven fluid dynamics, showed great promise to successfully produce 2D layered materials with higher yield.[55]

#### 3.1.2. Chemical Intercalation

The chemical intercalation of guest species to enlarge the interlayer spacing of bulk layered materials is a widely used technique for 2D material preparation (Figure 2b).[56] Chemical intercalation of graphite by strong oxidants results in GO, which is prepared first by covalently functionalizing the planar network of graphite via treatment of strong oxidants, such as sulfuric and nitric acid.[57] Graphite oxide, equipped with epoxide, hydroxyl, and carboxylic groups, is then exfoliated in water under mild sonication to output GO with yield over 90%.[58] GO is a water-soluble material that offers several opportunities for chemical modification.[59] However, the high density of defects due to the disruption of the conjugated graphitic network has a negative influence on the electrical properties.[60] Hence, extensive research on strategies to recover the conducting sp$^2$-carbon network have been carried out. To eliminate the oxygen-containing group from the GO structure several approaches have been investigated. Among them, chemical and thermal treatments are commonly used. Reducing agents such as hydrazine,[61] L-ascorbic acid,[62] and

**ADVANCED
SCIENCE NEWS**
www.advancedsciencenews.com

**ADVANCED
MATERIALS
TECHNOLOGIES**
www.advmattechnol.de
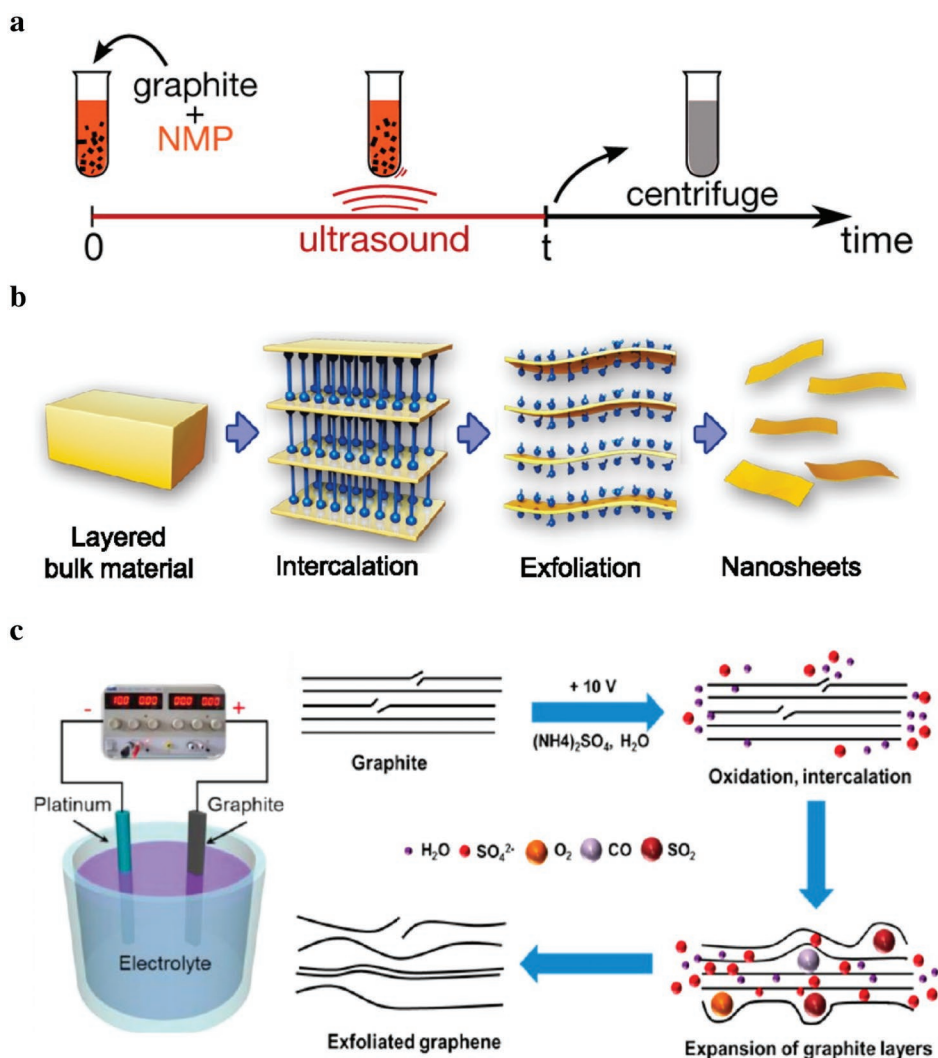
**Figure 2.** a) Schematic illustration of liquid-phase exfoliation. Reproduced with permission.[47] Copyright 2014, American Chemical Society. b) Illustrative scheme of chemical intercalation-assisted exfoliation of graphite. Reproduced with permission.[56] Copyright 2016, Springer Nature. c) Typical electrochemical cell for anodic exfoliation of graphite (left) and the related proposed exfoliation mechanism. Reproduced with permission.[77] Copyright 2014, American Chemical Society.

sodium borohydride[63] are usually employed for chemical reduction of GO, which results in formation of rGO with electric conductivities up to ≈300 S cm$^{-1}$. Thermal reduction operates at temperatures higher than 300 °C under vacuum,[64] inert,[65] or reducing atmosphere.[66] The thermal treatment generates carbon monoxide and carbon dioxide gases by eliminating the oxygen-containing functional groups of GO. The thermally converted rGO at 1100 °C shows electric conductivity of 550 S cm$^{-1}$.[67] Furthermore, high mobility values exceeding 1000 cm$^2$ V$^{-1}$ s$^{-1}$ can be obtained upon a multiple step reduction (annealing at 300 °C followed by microwave irradiation at 1000 W).[68] Nevertheless, compared to pure graphene nanosheets, rGO is highly disordered with inferior quality due to the presence of defects caused by the oxidation step. In contrast, non-oxidative intercalation of alkali metals into graphite lead to almost defect-free graphene.[69] Potassium intercalation is carried out by vapor diffusion under vacuum at 100 °C. The obtained graphene flakes, with ≈60% in the form of monolayer

and bilayer, present an electric conductivity of 320 S cm$^{-1}$.[70] Non-oxidative intercalation is also extended to other 2D materials. For example, high-quality single-layered semiconducting TMDCs, such as MoS$_2$ and WS$_2$, can be obtained from their bulk precursors upon lithium (Li) intercalation.[71] However,

**Table 1.** Surface tension and boiling points of common solvents used for liquid-phase exfoliation of graphite.[48]

| Solvent | Surface tension [mJ m$^{-2}$] | Boiling point [°C] |
|---|---|---|
| N-Methyl-2-pyrrolidone (NMP) | 40 | 203 |
| γ-Butyrolactone (GBL) | 46.5 | 204 |
| N,N-Dimethylacetamide (DMAC) | 36.7 | 165 |
| N,N-Dimethylformamide (DMF) | 37.1 | 154 |
| Dimethylsulfoxide (DMSO) | 42.8 | 189 |
| Ortho-dichlorobenzene (ODCB) | 37 | 181 |

**ADVANCED
SCIENCE NEWS**

www.advancedsciencenews.com

**ADVANCED
MATERIALS
TECHNOLOGIES**

www.advmattechnol.de
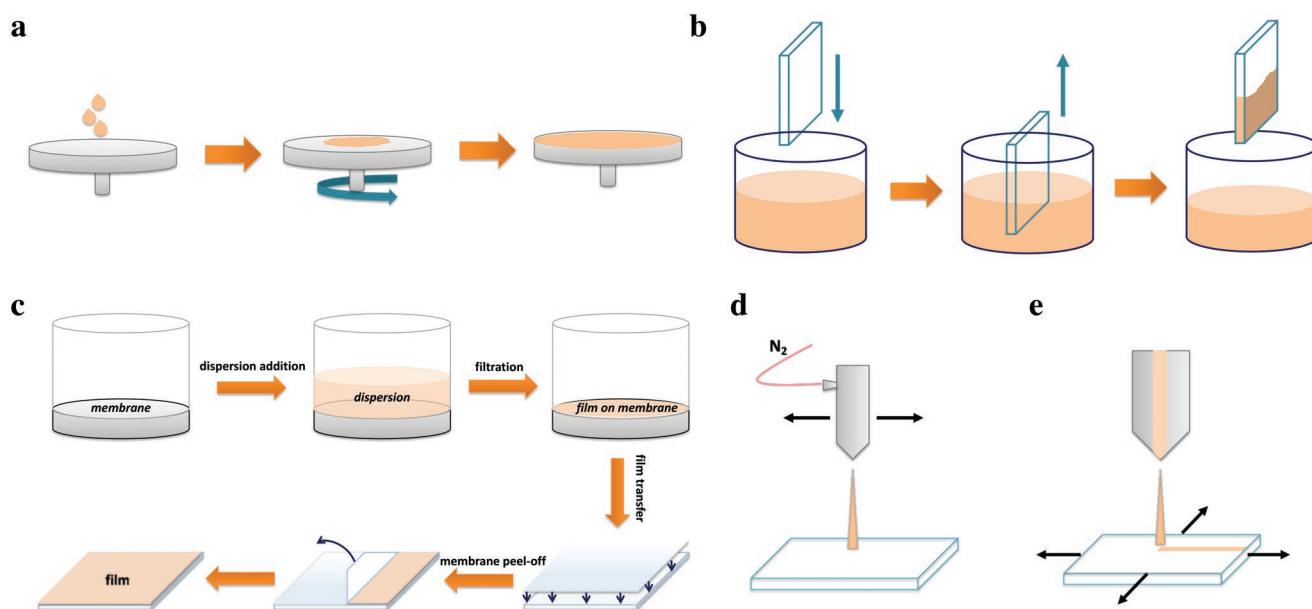
**Figure 3.** Schematic illustration of a) spin coating, b) dip coating, c) suction filtration, d) spray coating, and e) inkjet printing.

concerns on the hazardous Li-based compounds currently limit the large upscale.

### 3.1.3. Electrochemical Exfoliation

Electrochemical exfoliation of bulk layered materials has recently emerged as a promising strategy for 2D materials production.[72] Solution-processability, eco-friendliness, and upscalability are some of the advantages of this exfoliation method. In general, the exfoliation is driven upon the application of a voltage between a counter (i.e., platinum) and a working electrode (i.e., layered materials in the form of rods, foil, and plates) immersed into a conductive liquid media. The bulk material can undergo either anionic or cationic intercalation. Therefore, both anodic and cathodic exfoliation can be adopted.[73] The first is carried out in aqueous solution of inorganic salts or a mixture of water and ionic liquids.[74] For the latter organic solvents containing Li or quaternary salts are used.[75] In short, the general mechanism (Figure 2c) involves the intercalation of ions within the layers of the bulk material, followed by the formation of gaseous species, generated from solvent electrolysis, which expand the layers by overcoming the weak van der Waals forces.[76] Compared to other solution-processable routes, electrochemical exfoliation is ecofriendly (no hazardous reagents involved) and takes only few minutes to produce gram-scale quantities of high-quality 2D materials. Graphene can be produced in large quantities (yield > 80%) in aqueous solution of inorganic salts ($[NH_4]_2SO_4$, $Na_2SO_4$, $K_2SO_4$, etc.).[77] Anodic exfoliation of graphite in these electrolytes outputs ultrathin ($\approx$85% of one to three layer-thick flakes) large-area graphene flakes (up to 44 µm) with a hole mobility of as high as $\approx$300 cm$^2$ V$^{-1}$ s$^{-1}$. However, because of the generation of radicals (e.g., HO$^{\bullet}$) from the water electrolysis that inevitably causes defect formation on graphene, radical scavengers (e.g., (2,2,6,6-tetramethylpiperidin-1-yl)oxyl [TEMPO]) can be used.[10b] The controlled exfoliation leads to an enhancement

in hole mobility ($\approx$400 cm$^2$ V$^{-1}$ s$^{-1}$) as a consequence of the decreased amount of defects. Alternatively, a delamination strategy by using alternating currents between two graphitic electrodes can be employed to prevent defects.[78] High-quality graphene (C/O > 20) is yielded with a production rate of 20 g h$^{-1}$, which constitute a step forward toward industrial scalability. Electrochemical exfoliation has been successfully extended to BP.[79] Cathodic exfoliation of bulk BP in non-aqueous solvents with suitable intercalating agents (i.e., tetra-*n*-butylammonium cations) results in a high exfoliation yield up to 78%. Large BP flakes up to 20.6 µm with average thickness of 3.7 nm exhibit remarkable hole mobility of 252 cm$^2$ V$^{-1}$ s$^{-1}$. The electrochemical approach has also been demonstrated for TMDCs. For example, $MoS_2$ can be exfoliated in aqueous solution of $Na_2SO_4$.[80]

### 3.2. Processing Techniques of 2D Flakes for Optoelectronic Applications

The preparation of coatings used in the semiconductor industry relies mainly on vacuum deposition. Despite the high degree of film reproducibility and uniformity, vacuum methods experience large material consumption and high setup costs. Solution-processing techniques present various advantages such as reduced material waste, low costs, and high versatility. The performances of the final films are primarily influenced by both the nature of the dispersions and the parameters of the methods.[81] Hence, the choice of the right method is critical for film fabrication. The solution-processing strategies for 2D materials, with their advantages and disadvantages, are discussed in this paragraph.

### 3.2.1. Spin Coating

Spin coating (**Figure 3**a) is a conventional method to fabricate films for optoelectronic applications. The material, dispersed

**ADVANCED
SCIENCE NEWS**

www.advancedsciencenews.com

**ADVANCED
MATERIALS
TECHNOLOGIES**

www.advmattechnol.de

in a suitable solvent, is cast on top a substrate or previously coated films, which rotate at high speed. During this step, the dispersant is spread over the substrate due to the centripetal force. The coating of the material is then formed upon the evaporation of the solvent. The thickness of the film can be precisely controlled by tuning dispersion concentration, time and speed of the rotation. Despite the extremely fast, simple, and cost-effective approach, spin coating suffers from considerable waste of the material dispersion and limitations in fabrication of homogeneous large-area film.

### 3.2.2. Dip Coating

Thin-film coatings are commonly created by immersing and withdrawing a substrate into a dispersion (Figure 3b). The formation of the film occurs during the evaporation of the solvent after pulling the substrate out. Therefore, the sliding speed, the concentration of the dispersion, the viscosity, and the boiling point of the solvent play an important role in obtaining a uniform coverage. Simplicity, quickness, and reduced amount of material waste are some of the advantages of the dip-coating method. However, viscous solvents and multiple steps to form a film are often required. Moreover, double-side coating of substrates is inevitable, which leads to post-treatments to etch the back-side.

### 3.2.3. Suction Filtration

Freestanding films can be manufactured by using a vacuum pump to drive 2D material dispersions through a membrane (Figure 3c), which can be either hydrophilic or hydrophobic, according to the nature of the solvent. Further, 2D layered films can be transferred on top of a substrate by peeling the membrane off. In general, to increase the adhesion of the film, a mechanical press is used prior to the membrane removal. The thickness of the obtained coatings is controlled with the fine tuning of the concentration and volume of the dispersion. Suction filtration is a fast and simple coating method for small-area devices, since the size of the films depends on the filtration equipment.

### 3.2.4. Spray Coating

Spray coating is a deposition technique performed with an airbrush (Figure 3d). A carrier gas (i.e., nitrogen) pushes the dispersion droplets through the nozzle toward the substrate. Films are formed upon the evaporation of the solvent, which occurs in short time due to the large surface area of the drops. Spray coating is a convenient deposition method, suitable for large-area coatings on top of a wide selection of either flexible or rigid substrates. Film thickness and morphology is tuned by changing volume/concentration of the dispersion and pressure of the carrier gas. Moreover, masks can be employed to output specific patterns. Despite the remarkable versatility, manual operator errors might occur, reducing reproducibility for ultra-thin films. However, reproducibility on large scale can be enhanced by using automated systems.

### 3.2.5. Inkjet Printing

Inkjet printing is a non-contact printing technique, where ink droplets are jetted and deposited on the substrate with a specific programmed pattern, without the use of masks (Figure 3e). To get homogenous and high-performance coatings, many parameters regarding ink formulation, such as viscosity, stability, and rheological properties, need to be optimized. Commonly, high boiling point solvents are used to prepare 2D materials inks, which cause some hazardous concerns. Alternatively, surfactants are used in environmentally friendly solvents. As a drawback, additives residues often result in the deterioration of film performances.

## 4. General Overview of the Modern Organic and Perovskite Optoelectronics

Organic and perovskite semiconductors combine the electronic behavior of semiconductors, such as electrical conductivity, light absorption, and emission, with the ease of processing and chemical tunability, which open up endless possibilities in the field of optoelectronics. Notably, organic and perovskite optoelectronic applications such as SCs and LEDs have experienced a rapid growth, due to improved material design and physical understanding. In order to further enhance device performance, a proper design of their architectures and choice of materials are of primary importance. In this frame, the unique and diverse chemical and physical properties of 2D materials can be adopted to improve the efficacy of optoelectronic devices. As first step, the basic architecture and operation of these emerging SCs and LEDs will be discussed in this section.

### 4.1. Solar Cells

To date, the most commercialized and efficient SCs are based on inorganic materials such as silicon.[82] However, processing and cost of pure crystalline inorganic materials triggered an extensive research toward alternative photovoltaic modules. In contrast, organic and perovskite photovoltaics (PV) represent attractive emerging technologies, due to the low-cost and wide selection of the materials used in their modules.[83] Moreover, these emerging SCs allow compatibility with printing techniques and fabrication of semitransparent flexible devices.[84] Nevertheless, the actual OSCs and PeSCs market is hindered by different limitations. OSCs suffer from power conversion efficiencies (PCE) lower than their inorganic counterparts and lifetime limitations.[85] In contrast, perovskites, showing PCEs comparable to crystalline silicon (≈25%),[86] exhibit stability concerns.[87] Researchers are devoting many efforts to obtain highly efficient and stable organic and perovskite PV devices.[88] Recently, with the introduction of non-fullerene acceptors, encouraging results have been achieved for OSCs with PCE over 16%,[89] making OSCs commercialization more attractive. In parallel, more stable perovskite-based devices have been developed, by modifying their chemical composition and carrying out fundamental studies on the influence of the interfaces between perovskite and charge transport layers.[90]

**ADVANCED**
**SCIENCE NEWS**

www.advancedsciencenews.com

**ADVANCED**
**MATERIALS**
**TECHNOLOGIES**

www.advmattechnol.de
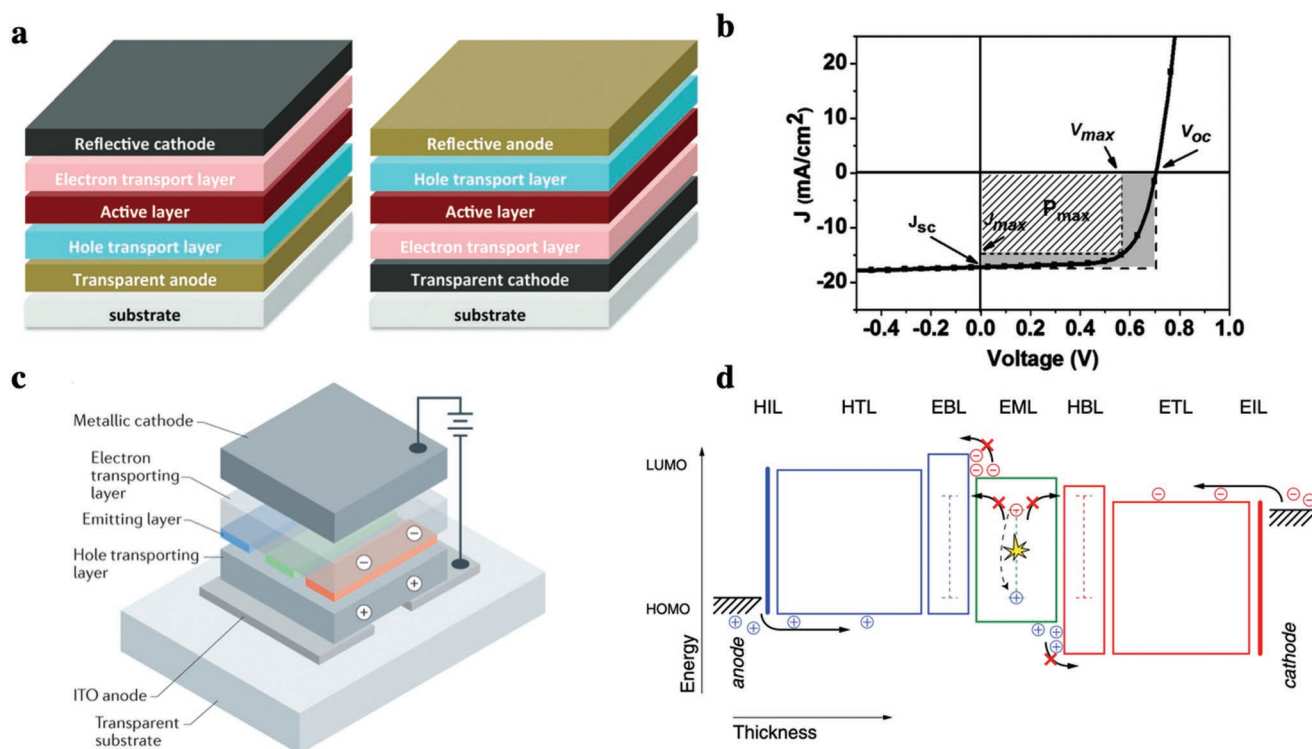
**Figure 4.** a) Schematic illustration of standard (left) and inverted (right) structure of OSCs. Reproduced with permission.[91] Copyright 2015, The Royal Society of Chemistry. b) Typical *J–V* characteristic of a solar cell. Reproduced with permission.[92] Copyright 2015, American Chemical Society. c) Schematic illustration of OLEDs. Reproduced with permission.[93] Copyright 2018, Springer Nature. d) Illustration of the charge behavior into an OLED with additional injection (I), transport (T), and blocking (B) layers. Reproduced with permission.[100] Copyright 2013, American Physical Society.

Both kinds of SCs have a vertical architecture in which the active layer is sandwiched between two electrodes. The typical setup is showed in **Figure 4**a.[91] The stack is deposited on a substrate (quartz or flexible polymer) covered with a transparent conductive electrode (TCE), which allows light transmission. The metal electrode, typically aluminum, gold, or silver, is commonly evaporated on top of the active layer. In addition, interfacial layers are often needed to optimize and balance the charge transport. The choice of the device components is based on the energy level alignment with the active layer.

The parameters to evaluate the performance of a SC are obtained by sweeping a voltage from negative to positive values in the dark and under illumination. The measurement leads to the current density–voltage (*J–V*) profile (Figure 4b), from which the PCE can be determined.[92]

### 4.2. Light-Emitting Diodes

LEDs are semiconductor devices that emit lights upon application of a voltage. High brightness, full-color capability, light weight, and low power consumption are just some of the superior features of the LEDs based on organic emitting materials.[93] Organic LEDs (OLEDs) consist of a vertical stack where the emitting material is embedded between two electrodes. Injection layers are often included between the electrodes and the emissive layer (Figure 4c) to enhance charge injection into the organic emitting layer.[93,94] While organic

LEDs have already hit the display market, perovskites are recently emerging as attractive light-emitting materials due to their remarkable optoelectronic properties, such as high absorption coefficients,[95] high color purity,[96] high PL quantum yield (PLQY),[97] and large hole and electron mobilities.[98] Indeed, in few years, perovskite LEDs (PeLEDs) have rapidly reached external quantum efficiency (EQE) values as high as 21.6%.[99] The basic working principle and device structure of PeLEDs are similar to the ones of an OLED.

The operation of an OLED relies mainly upon three features, which are charge injection, charge transport, and recombination, as shown in Figure 4d.[100] The EQE is the key parameter to evaluate the performance of a LED. The EQE is defined as the ratio between the number of emitted photons in the direction of the user and amount of injected carriers.

## 5. Practical Roles of 2D Materials in Organic and Perovskite Optoelectronics: Light-Emitting Diodes and Solar Cells

As previously described, LEDs and SCs consist in vertical stacks of components with distinct functionalities. Hence, 2D materials can be specifically employed in these devices according to their 2D nature. Indeed, the 2D family provides a diverse assortment of materials that matches the device requirements, with the aim of improving different operational aspects, such

**Table 2.** Key parameters of OSCs, PeSCs, and OLEDs based on solution-processed graphene TCEs.

| Device structure | $J_{sc}$ [mA cm$^{-2}$] | $V_{oc}$ [V] | FF | Luminance [cd m$^{-2}$] | PCE [%] | EQE [%] |
|---|---|---|---|---|---|---|
| rGO/CuPc/C$_{60}$/BCP/Ag[103] | 2.1 | 0.48 | 0.34 | – | 0.4 | – |
| rGO/PEDOT:PSS/P3HT:PCBM/TiO$_2$/Al[104] | 4.39 | 0.56 | 0.32 | | 0.78 | |
| rGO/PEDOT:PSS/P3HT:PCBM/LiF/Al[113] | 1.18 | 0.46 | 0.25 | – | 0.13 | – |
| rGO/PEDOT:PSS/P3HT:PCBM/Al[114] | 4.18 | 0.67 | 0.36 | – | 1.01 | – |
| rGO/PEDOT:PSS/ P3HT:PCBM/Al[115] | 5.56 | 0.57 | 0.32 | – | 1.01 | – |
| rGO/PEDOT:PSS/PCDTBT:PCBM/TiO$_2$/Al[105] | 7.81 | 0.85 | 0.46 | – | 3.05 | – |
| EG/PEDOT:PSS/PTB7:PCBM/Ba/Al[116] | 9.97 | 0.72 | 0.59 | – | 4.23 | – |
| EG-AgNWs/PEDOT:PSS/PTB7:PCBM/Ba/Al[112] | 15.5 | 0.73 | 0.58 | – | 6.57 | – |
| rGO/c-/m-TiO2/perovskite/spiro-OMeTAD/Au[117] | 3.05 | 0.69 | 0.38 | – | 0.81 | – |
| rGO/PEDOT:PSS/NPD/Alq3/LiF/Al[118] | – | – | – | 300 | – | – |
| GO-AgNWs/PEDOT:PSS/EL/PEI/GO-AgNWs[111] | – | – | – | 1100 | – | – |
| EG-AgNWs/PEDOT:PSS/SY/Ba/Al[112] | 105.7 | – | – | 104 25 | – | 4.4 |

as charge transport and extraction, interface stability, and performance. Furthermore, it is important to mention that the progress in 2D based SCs and LEDs is not solely due to the improvement of 2D materials, but also due to advanced device architectures and components. Therefore, care should be taken when comparing device efficiencies. In this section, the most common roles for solution-processed 2D materials are explored and described.

## 5.1. Transparent Electrodes

Indium tin oxide (ITO) is widely used as TCE in organic and perovskite optoelectronic devices, due to its remarkable optical and electrical properties.[101] As a drawback, ITO suffers from scarcity of supply, high production costs, and mechanical instability.[102] Among all the 2D materials, graphene has been proposed as an alternative TCE to ITO because of its attractive features, such as tunable work function (WF), high carrier mobility, and atomic-level thickness. However, a fundamental material limitation hinders this application. The sheet resistance $R_s$ of a monolayer of graphene amounts to only ≈6.4 kΩ sq$^{-1}$, which is much larger than typical values for ITO (≈10 Ω sq$^{-1}$).[20] Although multiple stacking of graphene leads to an improvement of $R_s$, its transmittance decreases with increasing amount of layers. For instance, three-layered graphene has a $R_s$ of ≈300 Ω sq$^{-1}$ and a transparency of 92%.[9a] To date, CVD graphene has led to the highest values in terms of conductivity and transmittance, which are beneficial for the final SCs and LEDs devices.[9a,42b] In contrast, the troublesome transfer process, especially for large-area architectures, the high cost, the presence of defects, and residues, limits the practical use of CVD graphene in commercial optoelectronics. Solution-processable approaches represent a fascinating option toward the scalability of graphene as TCE for real-market applications (**Table 2**). In addition to conductivity and transparency, morphology constitutes one of the key aspects for the successful implementation of 2D materials in either a SC or LED. Hence, to avoid short circuits or leakage pathways into the final device (thickness of few hundreds of nanometers), the films should be endowed

with low roughness and reduced amount of impurities. One of the first examples of a working OSC based on solution-processed graphene as TCE was described by Wu et al. in 2008 (**Figure 5**a).[103] The electrodes were deposited on quartz substrates by spin-coating an aqueous dispersion of GO, followed by a reduction step to decrease the $R_s$. Since the choice of the reduction process might lead to different rGO film conformations, either vacuum annealing at 1100 °C or combination of hydrazine treatment and argon (Ar) annealing at 400 °C was investigated. Both the approaches exhibited films with low roughness of the surface (<20 nm). The rGO TCEs showed $R_s$ values in a wide range spanning from 5 kΩ sq$^{-1}$ to 1 mΩ sq$^{-1}$ for films with transparencies higher than 80%. As result of the high $R_s$ and lower transmittance, rGO-based OSCs displayed much lower $J_{sc}$ and fill factor (FF) compared to the cell based on ITO, which inevitably resulted in lower PCE. To investigate the graphene behavior in flexible OSCs, rGO was deposited on polyethylene terephthalate (PET) by Yin et al.[104] First, GO was deposited on silicon oxide (SiO$_2$) substrates by spin-coating prior to reduction in Ar/hydrogen (H$_2$) at 1000 °C. Then, rGO was transferred onto poly(methyl methacrylate) (PMMA) and, successively, deposited on top of PET upon PMMA etching with acetone. The obtained flexible rGO electrodes exhibited $R_s$ values in the range of 16.0–1.6 kΩ sq$^{-1}$ for transparencies of 88% and 55%, respectively. Moreover, they exhibited a roughness of only ≈3 nm. The bulk heterojunction (BHJ) OSCs constituted of a blend of poly(3-hexylthiophene) (P3HT) as donor and phenyl-C$_{61}$-butyric acid methyl ester (PCBM) as acceptor, sandwiched between poly(3,4-ethylenedioxythiophene):poly(styrenesulfonate) (PEDOT:PSS) as hole transport layer (HTL) and titanium dioxide (TiO$_2$) as electron transport layer (ETL). In order to study the effect of rGO thickness on the performance of the OSCs, devices based on rGO films with different thickness were investigated. The optimal compromise between transparency and $R_s$ was found for an rGO film of 16 nm. Indeed, the PCE of the OSCs based on rGO TCE with $R_s$ and transmittance of 3.2 kΩ sq$^{-1}$ and 65%, respectively, was the highest among the set of devices. The mechanical performance of OSCs with an rGO-based electrode was studied by applying tensile stress on the devices. Bending tests of the flexible
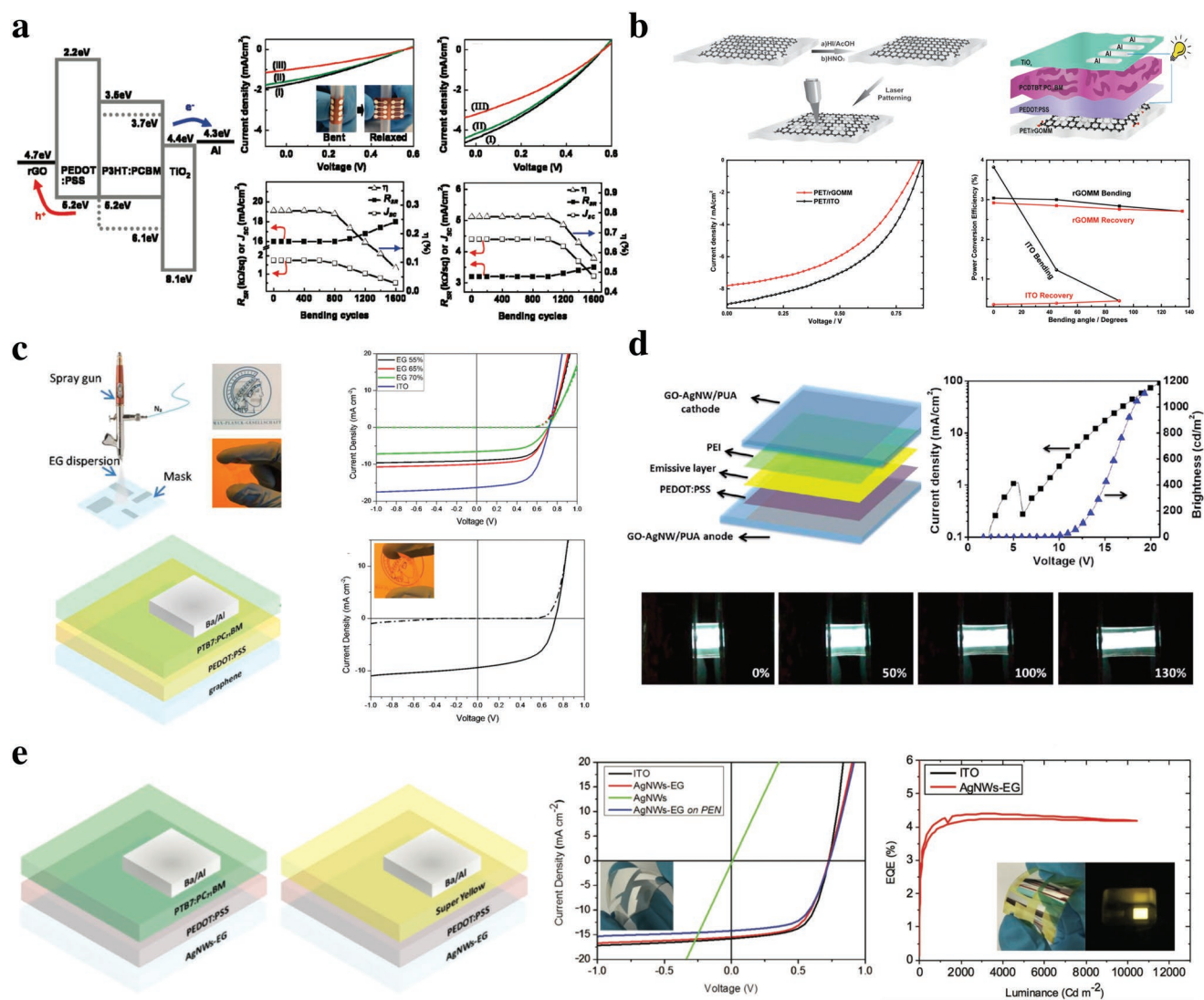
**Figure 5.** a) Band diagram of rGO-based OSCs (left) and PV performances under mechanical stress (right). Reproduced with permission.[104] Copyright 2010, American Chemical Society. b) Schematic illustration of the rGO mesh electrodes preparation (top left) and device architecture (top right). J–V characteristics of flexible OSCs (bottom left) and PCE behavior upon bending (bottom right) using rGO and ITO as TCE. Reproduced with permission.[105] Copyright 2015, Wiley-VCH. c) Schematic illustration of spray deposition of EG dispersion onto a substrate (top left). Inset: optical images of graphene TCE on both rigid and flexible substrates. OSCs architecture (bottom left) and J–V characteristics of rigid (top right) and flexible OPV devices (bottom right). Reproduced with permission.[116] Copyright 2017, American Chemical Society. d) Schematic illustration of stretchable OLED structure (top left) and its brightness behavior (top right). Stretching test under illumination (bottom). Reproduced with permission.[111] Copyright 2014, American Chemical Society. e) Devices architectures of SCs and LEDs based on AgNWs-EG bottom transparent electrode (left). J–V characteristics comparison of OSCs using ITO, pristine AgNWs, and AgNWs-EG TCEs (center). EQE of flexible LED (right). Inset: yellow-light emission of the AgNWs-EG flexible device. Reproduced with permission.[112] Copyright 2018, Wiley-VCH.

cells showed that degradation of the $J_{sc}$ and PCE occurred after 600 cycles. A different approach for flexible applications was used by Konios et al.[105] To improve the trade-off between conductivity and transmittance, rGO coatings on PET were patterned through a femtosecond laser treatment (Figure 5b). In particular, rGO films with an initial transparency of ≈20% were patterned, resulting in films with 59% transmittance and $R_s$ of 0.565 kΩ sq$^{-1}$, which is lower than the value of 0.780 kΩ sq$^{-1}$ exhibited by the pristine rGO TCE. The bending test demonstrated better stability of rGO-based flexible OSCs over ITO counterparts. Indeed, despite an initial higher performance

for the ITO-based device, its PCE significantly dropped after bending at ≈40°, due to crack formation.[106] In contrast, organic photovoltaic (OPV) devices endowed with rGO-based TCEs retained their photovoltaic performance after extreme bending. Recently, to further improve the $R_s$ values of graphene TCEs, electrochemical exfoliation of graphite was employed. Electrochemically exfoliated graphene (EG) was coated on top of either rigid or flexible substrates by spray-coating (Figure 5c), which provides fine control of the morphology. The coatings exhibited surface roughness as low as 2.86 nm and $R_s$ values ranging from 0.52 kΩ sq$^{-1}$ at 70% to 0.18 kΩ sq$^{-1}$ at 55%. The improved

**Table 3.** Key parameters of organic and perovskite devices employing 2D materials as HTLs and HILs.

| Device structure | $J_{sc}$ [mA cm$^{-2}$] | $V_{oc}$ [V] | FF | Luminance [cd m$^{-2}$] | PCE [%] | EQE [%] |
|---|---|---|---|---|---|---|
| 2D materials HTLs in OSCs | | | | | | |
| ITO/GO/P3HT:PCBM/Al[123] | 11.4 | 0.57 | 0.54 | – | 3.5 | – |
| ITO/GO–OSO$_3$H/P3HT:PCBM/Ca/Al[124] | 10.5 | 0.61 | 0.71 | – | 4.37 | – |
| ITO/rGO/PBDTTT-CF:PCBM/Ca/Al[125] | 15.3 | 0.75 | 0.63 | – | 7.18 | – |
| ITO/rGO/P3HT:PCBM/Ca/Al[139] | 9.33 | 0.59 | 0.67 | – | 3.63 | – |
| ITO/GO/PCDTBT:PC$_{71}$BM/TiO$_x$/Al[140] | 11.0 | 0.83 | 0.56 | – | 5.1 | – |
| ITO/GO/PTB7:PC$_{71}$BM/LiF/Al[141] | 15.2 | 0.72 | 0.68 | – | 7.39 | – |
| ITO/MoS$_x$/P3HT:PCBM/Ca/Al[131] | 9.96 | 0.58 | 0.67 | – | 3.90 | – |
| ITO/MoS$_2$/PEDOT:PSS/P3HT:PCBM/LiF/Al[132] | 7.97 | 0.52 | 0.68 | – | 2.81 | – |
| ITO/MOS$_2$/PTB7:PCBM/PFN/Al[142] | 15.0 | 0.73 | 0.70 | – | 7.64 | – |
| ITO/WS$_2$/PBDB-T-2F:Y6:PC$_{71}$BM/PFN-Br/Al[133] | 26.0 | 0.84 | 0.78 | – | 17.0 | – |
| 2D materials HTLs in PeSCs | | | | | | |
| FTO/TiO$_2$/CH$_3$NH$_3$PbI$_3$/rGO[143] | 16.7 | 0.94 | 0.73 | – | 11.5 | – |
| ITO/GO/CH$_3$NH$_3$PbI$_{3-x}$Cl$_x$/PCBM/ZnO/Al[126] | 17.46 | 1.00 | 0.71 | – | 12.4 | – |
| ITO/rGO/CH$_3$NH$_3$PbI$_3$/PC$_{61}$BM/BCP/Ag[127] | 14.81 | 0.95 | 0.71 | – | 10.8 | – |
| ITO/TiO$_2$/MAPbI$_3$Cl$_{3-x}$/rGO/spiroOMeTAD/Au[128] | 21.5 | 1.11 | 0.79 | – | 18.7 | – |
| ITO/MoS$_2$/CH$_3$NH$_3$PbI$_{3-x}$Cl$_x$/PCBM/BCP/LiF/Al[144] | 14.89 | 0.96 | 0.67 | – | 9.53 | – |
| ITO/PEDOT:PSS/MoS$_2$/CH$_3$NH$_3$PbI$_3$/PCBM/Ag[134a] | 24.03 | 1.00 | 0.69 | – | 16.5 | – |
| ITO/PEDOT:PSS/BP/CH$_3$NH$_3$PbI$_3$/PCBM/Ag[136] | 20.56 | 1.01 | 0.80 | – | 16.7 | – |
| 2D materials HILs in OLEDs and PeLEDs | | | | | | |
| ITO/GO/SY/LiF/Al[129] | – | – | – | 39 000 | – | 6.7 |
| ITO/rGO/TPD/Alq$_3$/Al[130] | – | – | – | 6232 | – | – |
| ITO/GO/TPD/Alq$_3$/Li$_3$N/Al[145] | – | – | – | 53 635 | – | 2.3 |
| ITO/MoS$_2$/NPB/Alq3:C545T/BCP/Alq$_3$/LiF/Al[135a] | – | – | – | 23 000 | – | – |
| ITO/PEDOT:PSS/BP/CsPbBr$_3$/TPBi/LiF/Al[138] | – | – | – | 20 636 | – | 2.8 |

values of $R_s$ are ascribed to the lower degree of defects of the EG. Indeed, as suggested by Raman spectroscopy, EG presented an $I_D/I_G$ ratio of 0.29, much smaller than that of rGO, typically in the range of 1.1–1.5.[107] As proof of concept, BHJ OSCs using poly[[4,8-bis[(2-ethylhexyl)oxy]benzo[1,2-b:4,5-b′]dithio-phene-2,6-diyl][3-fluoro-2-[(2-ethylhexy)carbonyl]thieno[3,4-b]thio-phenediyl]] (PTB7) and PCBM as donor and acceptor material, respectively, were fabricated. Despite the highest PCE reported for graphene-based electrodes (4.23%), the gap to the ITO-based counterparts (≈7%) still remains large because of higher $R_s$ values. Hence, to reduce the gap with well-established optoelectronic devices that rely on ITO, graphene was embedded with mono-dimensional (1D) materials such as silver nanowires (AgNWs). AgNWs show promising optical and electrical properties, such as high transmittance and conductivity.[108] However, AgNWs films exhibit several drawbacks, such as large contact resistance[109] and high surface roughness.[110] To overcome these limitations, hybrid TCEs of graphene and AgNWs were explored. The synergetic effect between these materials led to highly efficient flexible and stretchable optoelectronic devices. Bar-coated AgNW networks were soaked in GO solution to form a GO-soldered AgNW structure (Figure 5d).[111] The TCE had a figure-of-merit $R_s$ of 14 Ω sq$^{-1}$ with 88% transmittance, which is comparable to the one of the commercial ITO. The GO-AgNWs deposited on stretchable polyurethane acrylate film did not lose electrical conductivity upon linear strain. Fully stretchable and working white-light LEDs were fabricated employing the TCE as both the anode and cathode. Similarly, EG was used in combination of AgNWs for highly conductive TCEs for OSCs and OLEDs (Figure 5e).[112] The devices incorporating the solution-processed composite electrodes revealed similar behavior to the commercial ITO-based counterparts.

## 5.2. Hole Transport and Injection Layers

Polymers such as PEDOT:PSS and inorganic oxides are commonly used as hole injection layers (HILs) in OSCs and PeSCs and LEDs.[119] However, wetting and energy levels mismatch with subsequent layers may obviously occur for different systems, which limits their ubiquitous use. Moreover, PEDOT:PSS hygroscopic properties[120] and complicated inorganic oxides deposition methods contribute to the search for alternative HTLs and HILs.[121] 2D materials have been suggested as potential candidates for charge transport and injection layers for optoelectronics (**Table 3**). WF and wettability of graphene and its derivatives can be tuned by functionalizing their surface.[122] Thus, graphene can serve as a template to

**ADVANCED
SCIENCE NEWS**
www.advancedsciencenews.com

**ADVANCED
MATERIALS
TECHNOLOGIES**
www.advmattechnol.de

meet specific device requirements. GO was successfully used in P3HT:PCBM OSCs as HTL, delivering PCEs comparable to the one obtained with PEDOT:PSS (3.5%).[123] However, to improve both contact angle and conductivity, sulfated GO (GO-OSO$_3$H) was synthesized.[124] Indeed, pristine GO showed a contact angle of 36.5°. In contrast, sulfated GO, which is endowed with −OSO$_3$H groups attached to the carbon basal plane of rGO surrounded with edge-functionalized carboxyl groups, delivered higher contact angle (81.0°). As a consequence, even P3HT:PCBM coatings were formed. This was also confirmed by the higher FF of the OSCs, which improved from 0.58 to 0.71. In addition, WF of GO-OSO$_3$H (−4.8 eV) was deeper than that of GO, matching the highest occupied molecular orbital (HOMO) level of P3HT (−5.0 eV) for an ohmic contact. Hence, the overall efficiency of the OSCs using GO-OSO$_3$H as HTL was higher than the one with GO. Functionalization of graphene with sulfonic acid group constitutes a general route for high-performance HTLs in a wide selection of SCs with different photoactive layers. As a proof of concept, sulfonic acid-functionalized rGO has been integrated in OSCs with various donors, such as P3HT, PTB7, poly(2,3-bis(3-octyloxyphenyl)-5,8-quinoxalinediyl-2,5-thiophenediyl) (TQ1), and poly-1-(6-4,8-bis(2-ethylhexyl)oxy-6-methylbenzo1,2-b:4,5-b′dithiophen-2-yl-3-fluoro-4-methylthieno-3,4-b-thiophen-2-yl)-1-octanone (PBDTTT-CF).[125] Functionalized rGO was easily spin-coated on top of ITO from concentrated water. The resulting films exhibited higher conductivity (3.18 S m$^{-1}$) and higher WF (−5.04 eV) than the pristine GO ones (1.14 S m$^{-1}$ and −4.66 eV, respectively). The higher WF facilitated the creation of an ohmic contact for hole injection into deep HOMO materials. Hence, OSCs using functionalized rGO as HTL delivered enhanced average PCEs (as high as 7.18% for PBDTTT-CF:PCBM OSC), outperforming also the devices with PEDOT:PSS. GO HTLs has been successfully employed in PeSCs. For instance, iodide/chloride mixed halide perovskite film grown on GO exhibited superior crystallization and high surface coverage ratio.[126] The enhanced hole extraction from the perovskite to GO delivered a maximum PCE of 12.4% (**Figure 6**a), which was much higher than the PEDOT:PSS reference module (9.3%). As for the OSCs, rGO films with higher WF than GO leads to higher performance in PeSCs too. Compared to PEDOT:PSS and GO references, PeSCs with rGO yielded higher PCE values due to higher rGO conductivity, easier charge collection with a retarded recombination, better energy levels alignment, and surface matching of perovskite phase with rGO.[127] The deposition of 2D materials as HTLs is basically governed by spin-coating. A different approach was used by Li et al., who used a spray technique to coat the perovskite with functionalized rGO.[128] The optical transparent and conductive coating of 4-fluorophenyl-hydrazine hydrochloride (4FPH)-functionalized rGO passivated the traps at the perovskite grain boundaries, acting as a surface modifier. Consequently, hole extraction was significantly enhanced by introduction of rGO-4FPH, which further contributed to an increase of the $V_{OC}$. The PeSC with inverted structure ITO/TiO$_2$/CH$_3$NH$_3$PbI$_3$Cl$_{3-x}$/rGO-4FPH/spiro-OMeTAD/Au exhibited a PCE of 18.75%. Next to the intensive investigations of graphene and its derivatives as hole-transport materials in SCs, also their use in OLEDs has been explored. When GO is

used as HIL in LEDs with Super Yellow (SY) as polymeric emissive layer (Figure 6b), both luminance (39 000 cd m$^{-2}$) and EQE (6.7%) are enhanced compared to the reference LEDs using standard PEDOT:PSS (33 800 cd m$^{-2}$ and 3.5%, respectively).[129] Also in this case, the improvement was mainly ascribed to the reduced injection barrier between GO and SY. Next to GO also rGO was implemented in OLEDs. Here, GO was first deposited on an ITO substrate by the Langmuir–Blodgett (LB) technique and subsequently reduced to rGO.[130] The well-ordered and thickness-controlled rGO films made with LB method resulted in OLEDs with higher performance than spin-coated rGO.

As mentioned above, graphene has been considered as an alternative 2D material for ITO replacement, due to the excellent optical transmittance and conductivity. However, also other 2D materials as TMDCs and BP have been extensively studied as candidates for charge transport and injection layers. Their optical and electronic properties can be simply tuned by changing layer thickness. Hence, suitable TMDCs and BP films can be finely designed according to the band structure of the components of SCs and LEDs. Different approaches have been used for TMDCs as HTL. Thermally decomposed MoS$_x$ films on top of ITO were fabricated via spin-coating of (NH$_4$)$_2$MoS$_4$ aqueous dispersion. However, to achieve improvement in P3HT:PCBM OSCs performances over PEDOT:PSS, high-temperature annealing of the MoS$_x$ films (300 °C) was required.[131] In contrast, UV-ozone treatment on MoS$_2$ induces surface modification by incorporating oxygen atoms into the structure, leading to better wettability for coating additional layers on the top and changes in WF. The devices built in work from Van Le et al. showed better PV performance for UV-ozone-treated samples than the references.[132] Recently, solution-processed few-layers WS$_2$ has been employed as HTL into a 17% efficient ternary BHJ PBDB-T-2F:(2,2′-((2Z,2′Z)-((12,13-bis(2-ethylhexyl)-3,9-diundecyl-12,13-dihydro-[1,2,5]thiadiazolo[3,4e]thieno[2,″30″:4′,5′]thieno[2′,3′:4,5]pyrrolo[3,2-g]thieno[2′,3′:4,5]thieno[3,2-b]indole-2,10-diyl)bis(methanylylidene))bis(5,6-difluoro-3-oxo-2,3-dihydro-1H-indene-2,1-diylidene))dimalononitrile) (Y6):PC$_{71}$BM-based OSC (Figure 6c).[133] Uniform coatings of one- to three-layered WS$_2$ were obtained, with calculated WF ranging from −5.2 to −5.7 eV. The superior PV behavior of ternary BHJ PBDB-T-2F:Y6:PC$_{71}$BM cells with WS$_2$ over conventional HTLs was mainly ascribed to the lower bimolecular recombination in WS$_2$-based devices. This was attributed to the higher WF, which enables improved charge collection, and the reduced surface energy. Few layered MoS$_2$ has been used in blends with other HTLs, such as spiro-OMeTAD or PEDOT:PSS, for enhancing hole extraction in PeSCs.[134] Composites of MoS$_2$ have been also successfully used for light-emitting devices. MoS$_2$ in combination with GO or MoO$_3$ serves as efficient HIL in OLEDs.[135]

Graphene and TMDCs investigations have run in parallel with the rise of organic optoelectronics. Hence, extensive studies on their practical application into optoelectronic devices occurred for OSCs and OLEDs. In contrast, BP, which recently emerged as competitor of other 2D materials for its stunning electronic properties, has been mainly explored for perovskite-based devices, which nowadays constitutes the fastest-advancing technology for SCs and LEDs. BP quantum dots (QDs) from liquid exfoliation have been used in planar hybrid PeSCs.[136] BP

**ADVANCED
SCIENCE NEWS**

www.advancedsciencenews.com

**ADVANCED
MATERIALS
TECHNOLOGIES**

www.advmattechnol.de
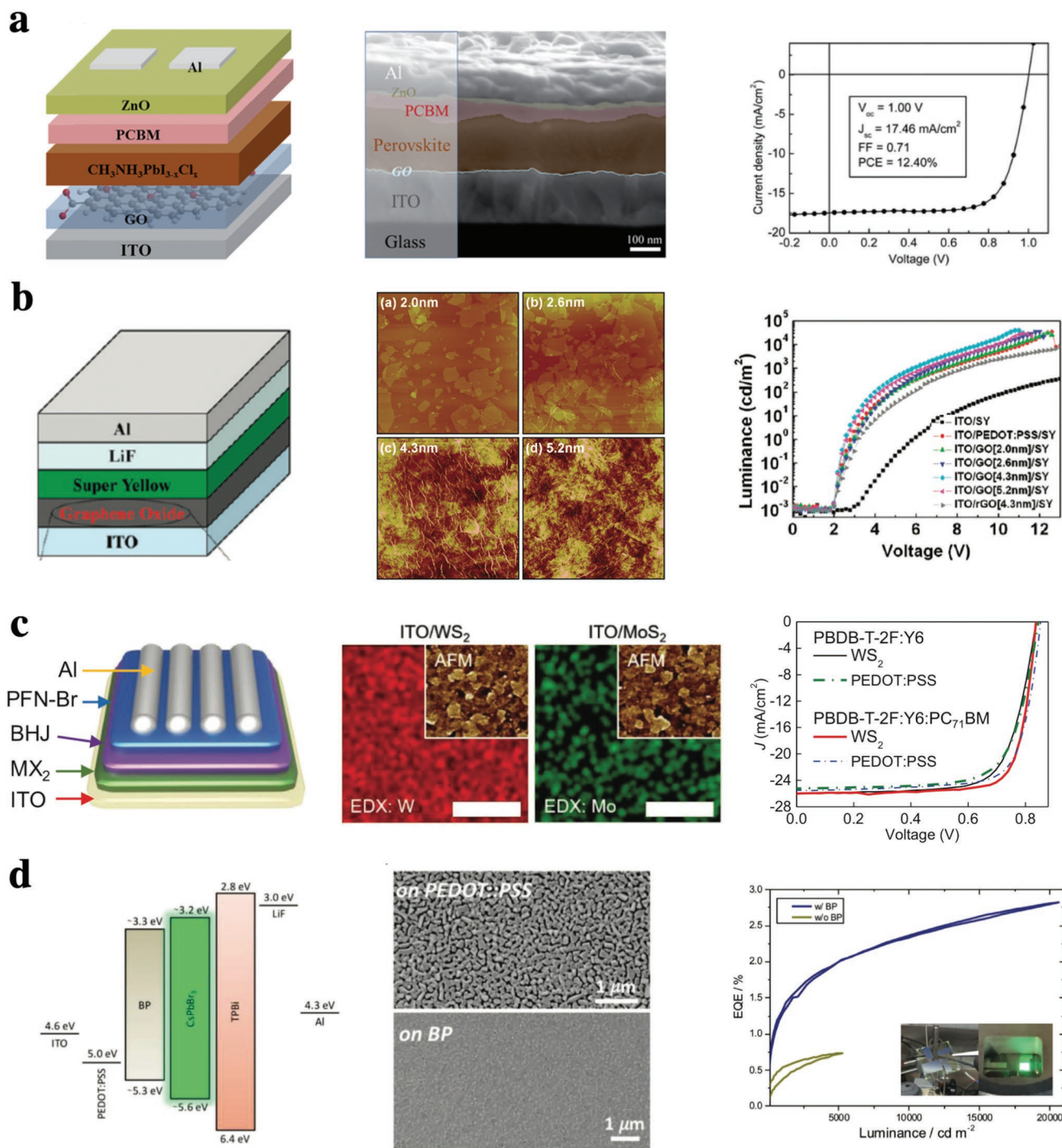
**Figure 6.** a) Schematic illustration of PeSC structure with GO as HTL (left) and cross-section scanning electron microscopy (SEM) image of the device (center). Best *J–V* characteristic of the PeSC (right). Reproduced with permission.[126] Copyright 2014, The Royal Society of Chemistry. b) Device schematics of LED with GO as HIL (left). Atomic force microscopy (AFM) images of different GO thicknesses (center). Luminance-*V* behavior of different set of devices (right). Reproduced with permission.[129] Copyright 2012, American Chemical Society. c) Schematic illustration of OSC endowed with WS$_2$ or MoS$_2$ as HTL (left). Elemental mapping of W and Mo from energy-dispersive X-ray spectroscopy (EDX) analysis on ITO/WS$_2$ and ITO/MoS$_2$, respectively. Insets show the corresponding AFM images of the films (center). *J–V* characteristics comparison for OSCs with standard PEDOT:PSS and WS$_2$ (right). Reproduced with permission.[133] Copyright 2019, Wiley-VCH. d) Energy band alignment diagram of PeSCs using BP as HIL (left). SEM morphology comparison of perovskite crystalline film on top of PEDOT:PSS and BP (center). EQE and luminance comparison between PeLEDs with and without BP. The inset shows the emitting device (right). Reproduced with permission.[138] Copyright 2018, Wiley-VCH.

**Table 4.** Key parameters of PeSCs and OSCs integrating 2D materials as HTL.

| Device structure | $J_{sc}$ [mA cm$^{-2}$] | $V_{oc}$ [V] | FF | PCE [%] |
|---|---|---|---|---|
| FTO/graphene-TiO$_2$/Al$_2$O$_3$/CH$_3$NH$_3$PBI$_{3-x}$Cl$_x$/spiroOMeTAD/Li-TFSI/Au[148] | 21.9 | 1.04 | 0.73 | 15.6 |
| FTO/TiO$_2$/graphene QDs/CH$_3$NH$_3$PbI$_3$/SpiroOMeTAD/Au[149] | 17.1 | 0.94 | 0.63 | 10.1 |
| ITO/WS$_2$/P3HT:PCBM/V$_2$O$_5$/Al[153] | 9.31 | 0.58 | 0.55 | 2.98 |
| ITO/MoS$_2$/P3HT:PCBM/V$_2$O$_5$/Al[153] | 11.2 | 0.58 | 0.52 | 3.35 |
| ITO/TaS$_2$/P3HT:PCBM/MoO$_3$/Al[150] | 8.76 | 0.60 | 0.52 | 2.73 |
| ITO/ZnO/BP/PTB7:PC$_{71}$BM/MoO$_3$/Ag[152] | 18.78 | 0.72 | 0.61 | 8.25 |

QDs were spin-coated on top of PEDOT:PSS, which improved the PCE of the PeSCs from 14.10% to 16.69%. Morphological and topological investigations revealed that BP QDs induce the growth of large grain size perovskite crystals. As evidenced by the hole-only devices, hole transport was improved with the presence of BP. Indeed, BP QDs had a lower WF (−5.1 eV) than PEDOT:PSS (−5.0 eV), closer to the VB of CH$_3$NH$_3$PBI$_3$ (−5.4 eV). However, BP has limited lateral size and abundance of defects, due to the long liquid-phase exfoliation.[137] Alternatively, electrochemical-exfoliated thin-layered and defect-free BP was employed as HIL in PeLEDs (Figure 6d) for reducing the injection barrier between PEDOT:PSS (−5.0 eV) and the emitting layer CsPbBr$_3$ (VB of −5.6 eV).[138] BP coatings with roughness of 8.0 nm were placed on top of PEDOT:PSS via mechanical deposition of vacuum filtered BP films. The entire process was carried out in ambient conditions due to the shell effect of the high boiling point solvent (DMF) used for dispersions. The integration of BP yielded ≈4 times luminance and EQE enhancement. The formation of pin-hole-free perovskite, as a consequence of better surface matching with BP, and enhanced hole injection, as confirmed by the hole-only devices, played a synergetic effect on the overall PeLED performance improvement.

### 5.3. Electron Transport and Injection Layers

The ambipolar behavior[146] and band structure engineering[147] make 2D materials, such graphene, TMDCs, and BP, also suitable for tuning the electron transport and injection. To date, only few works have been reported (**Table 4**), because surface mismatches lead to uneven coatings. Moreover, post-treatments (i.e., annealing) required for the 2D films and solvent used are often detrimental for the underlying components. Nanocomposites of intimately mixed liquid-phase EG and TiO$_2$ nanoparticles have been embedded in PeSCs (**Figure 7**a).[148] The authors observed reduced series resistance and recombination losses with the graphene-TiO$_2$ ETL, which delivered higher device performances (Figure 7b). Efficiency enhancement was found also by inserting a thin layer of graphene QDs between perovskite and TiO$_2$.[149] Transient absorption measurements revealed a faster electron extraction time of 90 ps as compared to 280 ps for devices with and without graphene QDs, respectively. Hence, graphene QDs are expected to work as superfast bridges for electron transfer from perovskite to TiO$_2$. TMDCs and BP have also been employed as ETLs in OPV. Van Le et al.

showed that OSCs with TaS$_2$ exhibit higher PCE than devices using TiO$_x$ as ETL (Figure 7c).[150] However, wide energy barrier between ETL and active layer still remained (Figure 7d). Alternatively, BP, similarly to the function of aryl phosphine oxide,[151] served to bridge the gap between the lowest unoccupied molecular orbital (LUMO) of PC$_{71}$BM (−3.7 eV) and the CB of ZnO (−4.2 eV) in OSCs with inverted structure (ITO/ZnO/BP/PTB7:PC$_{71}$BM/MoO$_3$/Ag), as shown in Figure 7e.[152] Indeed, 2D BP prepared in this work by intense sonication (average thickness of ≈10 nm), endowed with a LUMO of 3.86 eV, facilitated electron transport and contributed to the slight improvement of the PV performances (Figure 7f). Studies regarding the use of solution-processed 2D materials as EILs in LEDs are currently still missing.

## 6. Conclusion and Perspective

The research of the last years has shown that 2D materials have the ambition to serve as efficient optoelectronic device components. The diverse and remarkable optical and electric properties of 2D materials are suitable for many applications in OSCs and PeSCs and LEDs. It is worth noting that these technologies strongly rely on high performance at reduced costs to get into the consumer market. Therefore, to switch from emerging to well-established units of optoelectronic devices, high quality of the 2D materials at reasonable costs should be ensured. Solution-processable approaches for the synthesis of 2D materials meet all the requirements through ease of processing and cost effectiveness. Moreover, the recent progress in top-down exfoliation methods in solution has led to 2D materials with outstanding charge carrier mobility, conductivity, and optical transmittance.

Graphene, whether synthesized by CVD or solution methods, has been considered as intriguing alternative for ITO replacement for a long time. Although progress in this direction has been proven, due to selection of high-quality materials and post-treatment techniques (i.e., laser patterning), the use of graphene as standard TCE in optoelectronics is hindered by a fundamental limitation. The $R_s$ to transmittance ratio lags behind those of many alternatives (i.e., AgNWs and metal oxides). Therefore, it is more realistic to employ graphene as component of mixed-dimensional structures. This is the case of solution-processable graphene-metal NWs, which recently paved the way for practical TCE alternatives endowed with superior mechanical, electric, and optical properties. The conductive

**ADVANCED**
**SCIENCE NEWS**
www.advancedsciencenews.com

**ADVANCED**
**MATERIALS**
TECHNOLOGIES
www.advmattechnol.de
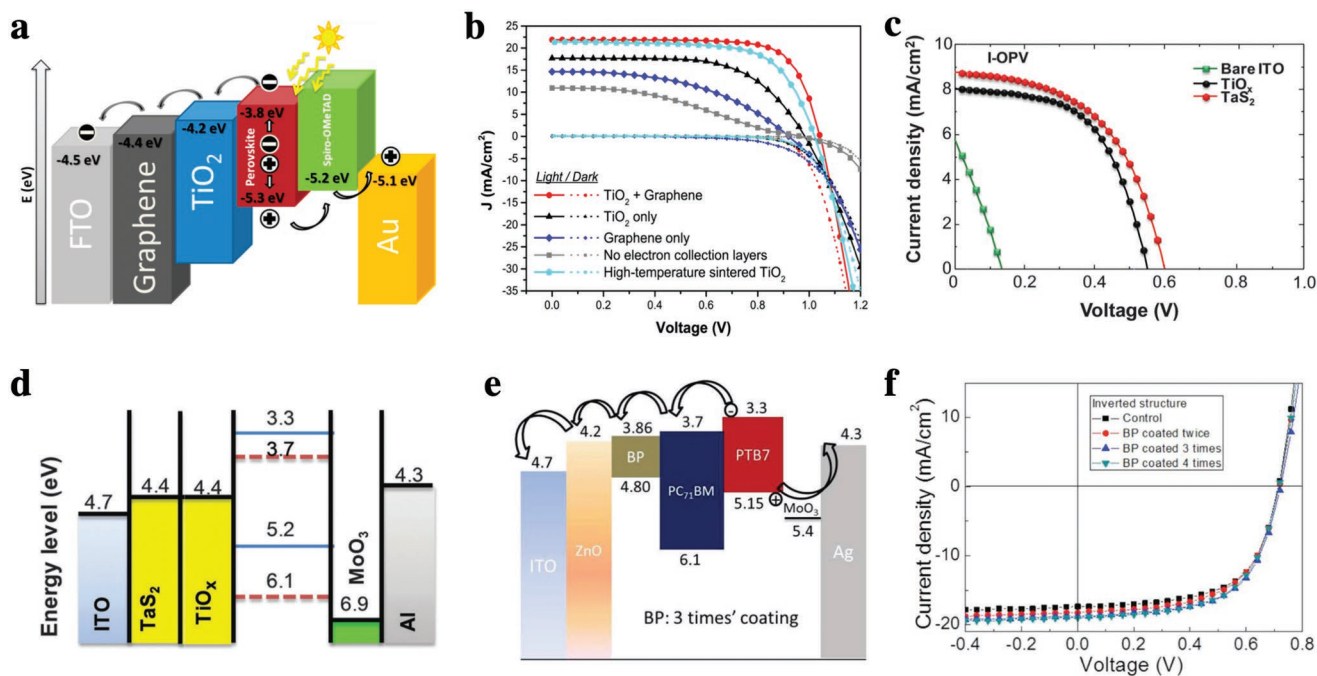
**Figure 7.** a) Schematic illustration of energy band structure of PeSCs with graphene-TiO₂ nanocomposite as ETL. b) *J–V* characteristics of various ETLs. Reproduced with permission.[148] Copyright 2013, American Chemical Society. c) Comparison of *J–V* characteristics of OSCs with TaS₂ and references. d) Schematic illustration of energy levels of the materials used. Reproduced with permission.[150] Copyright 2014, The Royal Society of Chemistry. e) Energy band structure of OPV device integrating BP. f) *J–V* characteristics of OSCs with different BP coating conditions. Reproduced with permission.[152] Copyright 2016, Wiley-VCH.

and mechanical/chemical stable matrix of thin-layered graphene plays an important role in reducing the limitation of the NWs, such as instability, detrimental high surface roughness, and large contact resistance. To fully exploit the strengths of 2D materials, other functions in SCs and LEDs can be explored. High carrier mobility, optical transparency, and stability are useful features for efficient charge transport and injection layers. Graphene films with specific wetting and electric properties can be finely tuned via chemical functionalization according to the device requirements, opening up endless possibilities. To date, many SCs and LEDs containing graphene-based charge transport and injection layers have outperformed traditional materials. Alternatively, TMDCs and BP exhibit a thickness-dependent band structure, which is a fascinating feature for designing versatile ubiquitous materials for optoelectronics. Both TMDCs and BP have been integrated in SCs and LEDs, showing better device behavior compared to standards. However, despite their great potential, only few studies that exploit their band gap tunability have been reported so far. The main issue lies in the lack of a reliable and facile route of obtaining a particular sheet thickness. Hence, more efforts toward the improvement of synthetic methods should be carried out in future. Despite the preliminary promising results, it is unlikely that 2D materials can be integrated as standard components in the state-of-the-art organic and perovskite optoelectronic devices within the next few years. Challenges regarding reproducibility, uniform properties distribution, and up-scaling are still unsolved. Nevertheless, in the long term, we believe that solution-processed 2D materials can be a regular asset of the next-generation optoelectronic devices. To achieve this goal, further studies in different fields should be performed, particularly, 1) synthesis optimization toward 2D defect-free sheets with larger size and uniform thickness distribution, which would generate improved electric properties; 2) deeper understanding of the structure to property relationships would help design tailored architectures for specific devices; 3) close cooperation between industry and academia for technical research and development and 4) integration of different nanostructured devices and systems such as photodetectors, transistors, and combined architectures for smart response and multifunctionalities.

## Conflict of Interest

The authors declare no conflict of interest.

## Keywords

[1] a) Y. F. Zhao, G. I. N. Waterhouse, G. B. Chen, X. Y. Xiong, L. Z. Wu, C. H. Tung, T. R. Zhang, *Chem. Soc. Rev.* **2019**, *48*, 1972; b) D. H. Deng, K. S. Novoselov, Q. Fu, N. F. Zheng, Z. Q. Tian, X. H. Bao, *Nat. Nanotechnol.* **2016**, *11*, 218.

**ADVANCED
SCIENCE NEWS**
www.advancedsciencenews.com

**ADVANCED
MATERIALS
TECHNOLOGIES**
www.advmattechnol.de

[2] a) F. Yi, H. Y. Ren, J. Y. Shan, X. Sun, D. Wei, Z. F. Liu, *Chem. Soc. Rev.* **2018**, *47*, 3152; b) Y. Q. Sun, Q. O. Wu, G. Q. Shi, *Energy Environ. Sci.* **2011**, *4*, 1113.

[3] a) M. F. El-Kady, Y. L. Shao, R. B. Kaner, *Nat. Rev. Mater.* **2016**, *1*, 14; b) K. S. Kumar, N. Choudhary, Y. Jung, J. Thomas, *ACS Energy Lett.* **2018**, *3*, 482; c) F. X. Wang, X. W. Wu, X. H. Yuan, Z. C. Liu, Y. Zhang, L. J. Fu, Y. S. Zhu, Q. M. Zhou, Y. P. Wu, W. Huang, *Chem. Soc. Rev.* **2017**, *46*, 6816.

[4] a) X. H. Liu, T. T. Ma, N. Pinna, J. Zhang, *Adv. Funct. Mater.* **2017**, *27*, 30; b) S. X. Yang, C. B. Jiang, S. H. Wei, *Appl. Phys. Rev.* **2017**, *4*, 021304.

[5] X. Zhou, X. Z. Hu, J. Yu, S. Y. Liu, Z. W. Shu, Q. Zhang, H. Q. Li, Y. Ma, H. Xu, T. Y. Zhai, *Adv. Funct. Mater.* **2018**, *28*, 28.

[6] S. L. Zhang, M. Q. Xie, F. Y. Li, Z. Yan, Y. F. Li, E. J. Kan, W. Liu, Z. F. Chen, H. B. Zeng, *Angew. Chem., Int. Ed.* **2016**, *55*, 1666.

[7] X. D. Duan, C. Wang, A. L. Pan, R. Q. Yu, X. F. Duan, *Chem. Soc. Rev.* **2015**, *44*, 8859.

[8] Y. Liu, N. O. Weiss, X. D. Duan, H. C. Cheng, Y. Huang, X. F. Duan, *Nat. Rev. Mater.* **2016**, *1*, 17.

[9] a) H. Park, S. Chang, X. Zhou, J. Kong, T. Palacios, S. Gradečak, *Nano Lett.* **2014**, *14*, 5148; b) K. C. Kwon, C. Kim, Q. V. Le, S. Gim, J.-M. Jeon, J. Y. Ham, J.-L. Lee, H. W. Jang, S. Y. Kim, *ACS Nano* **2015**, *9*, 4146; c) Y. Yang, J. Gao, Z. Zhang, S. Xiao, H. H. Xie, Z. B. Sun, J. H. Wang, C. H. Zhou, Y. W. Wang, X. Y. Guo, P. K. Chu, X. F. Yu, *Adv. Mater.* **2016**, *28*, 8937.

[10] a) Z. Lin, Y. Liu, U. Halim, M. Ding, Y. Liu, Y. Wang, C. Jia, P. Chen, X. Duan, C. Wang, F. Song, M. Li, C. Wan, Y. Huang, X. Duan, *Nature* **2018**, *562*, 254; b) S. Yang, S. Brüller, Z.-S. Wu, Z. Liu, K. Parvez, R. Dong, F. Richard, P. Samorì, X. Feng, K. Müllen, *J. Am. Chem. Soc.* **2015**, *137*, 13927.

[11] a) A. K. Geim, K. S. Novoselov, *Nat. Mater.* **2007**, *6*, 183; b) F. Xia, H. Wang, D. Xiao, M. Dubey, A. Ramasubramaniam, *Nat. Photonics* **2014**, *8*, 899.

[12] A. H. Castro Neto, F. Guinea, N. M. R. Peres, K. S. Novoselov, A. K. Geim, *Rev. Mod. Phys.* **2009**, *81*, 109.

[13] S. Thongrattanasiri, F. H. L. Koppens, F. J. G. de Abajo, *Phys. Rev. Lett.* **2012**, *108*, 5.

[14] a) O. V. Yazyev, Y. P. Chen, *Nat. Nanotechnol.* **2014**, *9*, 755; b) O. V. Yazyev, S. G. Louie, *Nat. Mater.* **2010**, *9*, 806.

[15] a) A. Lherbier, X. Blase, Y.-M. Niquet, F. Triozon, S. Roche, *Phys. Rev. Lett.* **2008**, *101*, 036808; b) H. Liu, Y. Liu, D. Zhu, *J. Mater. Chem.* **2011**, *21*, 3335.

[16] a) H. Zhang, E. Bekyarova, J.-W. Huang, Z. Zhao, W. Bao, F. Wang, R. C. Haddon, C. N. Lau, *Nano Lett.* **2011**, *11*, 4047; b) J. Son, S. Lee, S. J. Kim, B. C. Park, H.-K. Lee, S. Kim, J. H. Kim, B. H. Hong, J. Hong, *Nat. Commun.* **2016**, *7*, 13261.

[17] a) Y. W. Son, M. L. Cohen, S. G. Louie, *Phys. Rev. Lett.* **2006**, *97*, 4; b) J. W. Bai, X. Zhong, S. Jiang, Y. Huang, X. F. Duan, *Nat. Nanotechnol.* **2010**, *5*, 190.

[18] J.-H. Chen, C. Jang, S. Xiao, M. Ishigami, M. S. Fuhrer, *Nat. Nanotechnol.* **2008**, *3*, 206.

[19] K. S. Novoselov, V. I. Fal'ko, L. Colombo, P. R. Gellert, M. G. Schwab, K. Kim, *Nature* **2012**, *490*, 192.

[20] F. Bonaccorso, Z. Sun, T. Hasan, A. C. Ferrari, *Nat. Photonics* **2010**, *4*, 611.

[21] D. Chen, H. Feng, J. Li, *Chem. Rev.* **2012**, *112*, 6027.

[22] a) Z. Sun, H. Chang, *ACS Nano* **2014**, *8*, 4133; b) K. P. Loh, S. W. Tong, J. Wu, *J. Am. Chem. Soc.* **2016**, *138*, 1095.

[23] A. L. Higginbotham, D. V. Kosynkin, A. Sinitskii, Z. Sun, J. M. Tour, *ACS Nano* **2010**, *4*, 2059.

[24] H. Kinoshita, I. Jeon, M. Maruyama, K. Kawahara, Y. Terao, D. Ding, R. Matsumoto, Y. Matsuo, S. Okada, H. Ago, *Adv. Mater.* **2017**, *29*, 1702141.

[25] H. Liu, A. T. Neal, Z. Zhu, Z. Luo, X. Xu, D. Tománek, P. D. Ye, *ACS Nano* **2014**, *8*, 4033.

[26] L. Li, Y. Yu, G. J. Ye, Q. Ge, X. Ou, H. Wu, D. Feng, X. H. Chen, Y. Zhang, *Nat. Nanotechnol.* **2014**, *9*, 372.

[27] F. Xia, H. Wang, Y. Jia, *Nat. Commun.* **2014**, *5*, 4458.

[28] J. Qiao, X. Kong, Z.-X. Hu, F. Yang, W. Ji, *Nat. Commun.* **2014**, *5*, 4475.

[29] S. Huang, X. Ling, *Small* **2017**, *13*, 1700823.

[30] Y. Liu, T. Low, P. P. Ruden, *Phys. Rev. B* **2016**, *93*, 165402.

[31] Y. Xu, Z. Shi, X. Shi, K. Zhang, H. Zhang, *Nanoscale* **2019**, *11*, 14491.

[32] V. Tran, R. Soklaski, Y. Liang, L. Yang, *Phys. Rev. B* **2014**, *89*, 235319.

[33] A. N. Rudenko, M. I. Katsnelson, *Phys. Rev. B* **2014**, *89*, 201408.

[34] a) J. A. Wilson, A. D. Yoffe, *Adv. Phys.* **1969**, *18*, 193; b) L. F. Mattheiss, *Phys. Rev. B* **1973**, *8*, 3719.

[35] S. Manzeli, D. Ovchinnikov, D. Pasquier, O. V. Yazyev, A. Kis, *Nat. Rev. Mater.* **2017**, *2*, 17033.

[36] B. Radisavljevic, A. Radenovic, J. Brivio, V. Giacometti, A. Kis, *Nat. Nanotechnol.* **2011**, *6*, 147.

[37] Q. H. Wang, K. Kalantar-Zadeh, A. Kis, J. N. Coleman, M. S. Strano, *Nat. Nanotechnol.* **2012**, *7*, 699.

[38] A. Kuc, N. Zibouche, T. Heine, *Phys. Rev. B* **2011**, *83*, 245213.

[39] K. F. Mak, C. Lee, J. Hone, J. Shan, T. F. Heinz, *Phys. Rev. Lett.* **2010**, *105*, 136805.

[40] X. Li, J. T. Mullen, Z. Jin, K. M. Borysenko, M. Buongiorno Nardelli, K. W. Kim, *Phys. Rev. B* **2013**, *87*, 115418.

[41] Z. Yu, Z.-Y. Ong, S. Li, J.-B. Xu, G. Zhang, Y.-W. Zhang, Y. Shi, X. Wang, *Adv. Funct. Mater.* **2017**, *27*, 1604093.

[42] a) A. Reina, X. T. Jia, J. Ho, D. Nezich, H. B. Son, V. Bulovic, M. S. Dresselhaus, J. Kong, *Nano Lett.* **2009**, *9*, 30; b) Y. Wang, S. W. Tong, X. F. Xu, B. Özyilmaz, K. P. Loh, *Adv. Mater.* **2011**, *23*, 1514.

[43] a) L. Gao, G.-X. Ni, Y. Liu, B. Liu, A. H. Castro Neto, K. P. Loh, *Nature* **2014**, *505*, 190; b) L. Lin, H. Peng, Z. Liu, *Nat. Mater.* **2019**, *18*, 520.

[44] K. R. Paton, E. Varrla, C. Backes, R. J. Smith, U. Khan, A. O'Neill, C. Boland, M. Lotya, O. M. Istrate, P. King, T. Higgins, S. Barwich, P. May, P. Puczkarski, I. Ahmed, M. Moebius, H. Pettersson, E. Long, J. Coelho, S. E. O'Brien, E. K. McGuire, B. M. Sanchez, G. S. Duesberg, N. McEvoy, T. J. Pennycook, C. Downing, A. Crossley, V. Nicolosi, J. N. Coleman, *Nat. Mater.* **2014**, *13*, 624.

[45] D. Hanlon, C. Backes, E. Doherty, C. S. Cucinotta, N. C. Berner, C. Boland, K. Lee, A. Harvey, P. Lynch, Z. Gholamvand, S. Zhang, K. Wang, G. Moynihan, A. Pokle, Q. M. Ramasse, N. McEvoy, W. J. Blau, J. Wang, G. Abellan, F. Hauke, A. Hirsch, S. Sanvito, D. D. O'Regan, G. S. Duesberg, V. Nicolosi, J. N. Coleman, *Nat. Commun.* **2015**, *6*, 8563.

[46] J. N. Coleman, M. Lotya, A. O'Neill, S. D. Bergin, P. J. King, U. Khan, K. Young, A. Gaucher, S. De, R. J. Smith, I. V. Shvets, S. K. Arora, G. Stanton, H.-Y. Kim, K. Lee, G. T. Kim, G. S. Duesberg, T. Hallam, J. J. Boland, J. J. Wang, J. F. Donegan, J. C. Grunlan, G. Moriarty, A. Shmeliov, R. J. Nicholls, J. M. Perkins, E. M. Grieveson, K. Theuwissen, D. W. McComb, P. D. Nellist, V. Nicolosi, *Science* **2011**, *331*, 568.

[47] M. V. Bracamonte, G. I. Lacconi, S. E. Urreta, L. E. F. Foa Torres, *J. Phys. Chem. C* **2014**, *118*, 15455.

[48] Y. Xu, H. Cao, Y. Xue, B. Li, W. Cai, *Nanomaterials* **2018**, *8*, 942.

[49] J. N. Coleman, *Adv. Funct. Mater.* **2009**, *19*, 3680.

[50] J. N. Coleman, *Acc. Chem. Res.* **2013**, *46*, 14.

[51] Y. Hernandez, V. Nicolosi, M. Lotya, F. M. Blighe, Z. Sun, S. De, I. T. McGovern, B. Holland, M. Byrne, Y. K. Gun'Ko, J. J. Boland, P. Niraj, G. Duesberg, S. Krishnamurthy, R. Goodhue, J. Hutchison, V. Scardaci, A. C. Ferrari, J. N. Coleman, *Nat. Nanotechnol.* **2008**, *3*, 563.

[52] a) U. Halim, C. R. Zheng, Y. Chen, Z. Lin, S. Jiang, R. Cheng, Y. Huang, X. Duan, *Nat. Commun.* **2013**, *4*, 2213; b) M. Yi, Z. G. Shen, S. L. Ma, X. J. Zhang, *J. Nanopart. Res.* **2012**, *14*, 9.

[53] M. Lotya, Y. Hernandez, P. J. King, R. J. Smith, V. Nicolosi, L. S. Karlsson, F. M. Blighe, S. De, Z. Wang, I. T. McGovern, G. S. Duesberg, J. N. Coleman, *J. Am. Chem. Soc.* **2009**, *131*, 3611.

[54] A. Ciesielski, P. Samorì, *Chem. Soc. Rev.* **2014**, *43*, 381.

[55] a) S. Biccai, S. Barwich, D. Boland, A. Harvey, D. Hanlon, N. McEvoy, J. N. Coleman, *2D Mater.* **2018**, *6*, 015008; b) P. G. Karagiannidis, S. A. Hodge, L. Lombardi, F. Tomarchio, N. Decorde, S. Milana, I. Goykhman, Y. Su, S. V. Mesite, D. N. Johnstone, R. K. Leary, P. A. Midgley, N. M. Pugno, F. Torrisi, A. C. Ferrari, *ACS Nano* **2017**, *11*, 2742.

[56] Z. Sun, T. Liao, L. Kou, *Sci. China Mater.* **2017**, *60*, 1.

[57] W. S. Hummers, R. E. Offeman, *J. Am. Chem. Soc.* **1958**, *80*, 1339.

[58] a) Z. Luo, Y. Lu, L. A. Somers, A. T. C. Johnson, *J. Am. Chem. Soc.* **2009**, *131*, 898; b) N. M. Huang, H. N. Lim, C. H. Chia, M. A. Yarmo, M. R. Muhamad, *Int. J. Nanomed.* **2011**, *6*, 3443.

[59] J. Liu, J. Tang, J. J. Gooding, *J. Mater. Chem.* **2012**, *22*, 12435.

[60] M. Cheng, R. Yang, L. Zhang, Z. Shi, W. Yang, D. Wang, G. Xie, D. Shi, G. Zhang, *Carbon* **2012**, *50*, 2581.

[61] S. Stankovich, D. A. Dikin, R. D. Piner, K. A. Kohlhaas, A. Kleinhammes, Y. Jia, Y. Wu, S. T. Nguyen, R. S. Ruoff, *Carbon* **2007**, *45*, 1558.

[62] J. Zhang, H. Yang, G. Shen, P. Cheng, J. Zhang, S. Guo, *Chem. Commun.* **2010**, *46*, 1112.

[63] H.-J. Shin, K. K. Kim, A. Benayad, S.-M. Yoon, H. K. Park, I.-S. Jung, M. H. Jin, H.-K. Jeong, J. M. Kim, J.-Y. Choi, Y. H. Lee, *Adv. Funct. Mater.* **2009**, *19*, 1987.

[64] H. A. Becerril, J. Mao, Z. Liu, R. M. Stoltenberg, Z. Bao, Y. Chen, *ACS Nano* **2008**, *2*, 463.

[65] D. Yang, A. Velamakanni, G. Bozoklu, S. Park, M. Stoller, R. D. Piner, S. Stankovich, I. Jung, D. A. Field, C. A. Ventrice, R. S. Ruoff, *Carbon* **2009**, *47*, 145.

[66] X. Li, H. Wang, J. T. Robinson, H. Sanchez, G. Diankov, H. Dai, *J. Am. Chem. Soc.* **2009**, *131*, 15939.

[67] X. Wang, L. Zhi, K. Müllen, *Nano Lett.* **2008**, *8*, 323.

[68] D. Voiry, J. Yang, J. Kupferberg, R. Fullon, C. Lee, H. Y. Jeong, H. S. Shin, M. Chhowalla, *Science* **2016**, *353*, 1413.

[69] K. H. Park, D. Lee, J. Kim, J. Song, Y. M. Lee, H.-T. Kim, J.-K. Park, *Nano Lett.* **2014**, *14*, 4306.

[70] G. Bepete, E. Anglaret, L. Ortolani, V. Morandi, K. Huang, A. Pénicaud, C. Drummond, *Nat. Chem.* **2017**, *9*, 347.

[71] a) V. Nicolosi, M. Chhowalla, M. G. Kanatzidis, M. S. Strano, J. N. Coleman, *Science* **2013**, *340*, 1226419; b) G. Eda, H. Yamaguchi, D. Voiry, T. Fujita, M. Chen, M. Chhowalla, *Nano Lett.* **2011**, *11*, 5111; c) G. Eda, T. Fujita, H. Yamaguchi, D. Voiry, M. Chen, M. Chhowalla, *ACS Nano* **2012**, *6*, 7311.

[72] a) S. Yang, M. R. Lohe, K. Müllen, X. Feng, *Adv. Mater.* **2016**, *28*, 6213; b) S. Yang, P. Zhang, F. Wang, A. G. Ricciardulli, M. R. Lohe, P. W. M. Blom, X. Feng, *Angew. Chem., Int. Ed.* **2018**, *57*, 15491.

[73] C. T. J. Low, F. C. Walsh, M. H. Chakrabarti, M. A. Hashim, M. A. Hussain, *Carbon* **2013**, *54*, 1.

[74] a) C.-Y. Su, A.-Y. Lu, Y. Xu, F.-R. Chen, A. N. Khlobystov, L.-J. Li, *ACS Nano* **2011**, *5*, 2332; b) V. V. Singh, G. Gupta, A. Batra, A. K. Nigam, M. Boopathi, P. K. Gutch, B. K. Tripathi, A. Srivastava, M. Samuel, G. S. Agarwal, B. Singh, R. Vijayaraghavan, *Adv. Funct. Mater.* **2012**, *22*, 2352.

[75] K. Parvez, S. Yang, X. L. Feng, K. Mullen, *Synth. Met.* **2015**, *210*, 123.

[76] K. Parvez, R. Li, S. R. Puniredd, Y. Hernandez, F. Hinkel, S. Wang, X. Feng, K. Müllen, *ACS Nano* **2013**, *7*, 3598.

[77] K. Parvez, Z.-S. Wu, R. Li, X. Liu, R. Graf, X. Feng, K. Müllen, *J. Am. Chem. Soc.* **2014**, *136*, 6083.

[78] S. Yang, A. G. Ricciardulli, S. Liu, R. Dong, M. R. Lohe, A. Becker, M. A. Squillaci, P. Samorì, K. Müllen, X. Feng, *Angew. Chem., Int. Ed.* **2017**, *56*, 6669.

[79] S. Yang, K. Zhang, A. G. Ricciardulli, P. Zhang, Z. Liao, M. R. Lohe, E. Zschech, P. W. M. Blom, W. Pisula, K. Müllen, X. Feng, *Angew. Chem., Int. Ed.* **2018**, *57*, 4677.

[80] N. Liu, P. Kim, J. H. Kim, J. H. Ye, S. Kim, C. J. Lee, *ACS Nano* **2014**, *8*, 6902.

[81] X. Cai, Y. Luo, B. Liu, H.-M. Cheng, *Chem. Soc. Rev.* **2018**, *47*, 6224.

[82] I. van Beuzekom, B. M. Hodge, H. Slootweg, in *2018 IEEE Int. Energy Conf. (ENERGYCON)*, IEEE, Piscataway **2018**, pp. 1–6.

[83] a) A. Wadsworth, M. Moser, A. Marks, M. S. Little, N. Gasparini, C. J. Brabec, D. Baran, I. McCulloch, *Chem. Soc. Rev.* **2019**, *48*, 1596; b) F. Huang, M. J. Li, P. Siffalovic, G. Z. Cao, J. J. Tian, *Energy Environ. Sci.* **2019**, *12*, 518.

[84] a) K. Sun, Z. Y. Xiao, S. R. Lu, W. Zajaczkowski, W. Pisula, E. Hanssen, J. M. White, R. M. Williamson, J. Subbiah, J. Y. Ouyang, A. B. Holmes, W. W. H. Wong, D. J. Jones, *Nat. Commun.* **2015**, *6*, 9; b) W. Wu, *Nanoscale* **2017**, *9*, 7342.

[85] a) Q. Burlingame, X. H. Huang, X. Liu, C. Jeong, C. Coburn, S. R. Forrest, *Nature* **2019**, *573*, 394; b) Y. Cui, H. F. Yao, L. Hong, T. Zhang, Y. Xu, K. Hian, B. W. Gao, J. Z. Qin, J. Q. Zhang, Z. X. Wei, J. H. Hou, *Adv. Mater.* **2019**, *31*, 7.

[86] R. Lin, K. Xiao, Z. Qin, Q. Han, C. Zhang, M. Wei, M. I. Saidaminov, Y. Gao, J. Xu, M. Xiao, A. Li, J. Zhu, E. H. Sargent, H. Tan, *Nat. Energy* **2019**, *4*, 864.

[87] C. C. Boyd, R. Cheacharoen, T. Leijtens, M. D. McGehee, *Chem. Rev.* **2019**, *119*, 3418.

[88] E. H. Jung, N. J. Jeon, E. Y. Park, C. S. Moon, T. J. Shin, T.-Y. Yang, J. H. Noh, J. Seo, *Nature* **2019**, *567*, 511.

[89] B. Fan, D. Zhang, M. Li, W. Zhong, Z. Zeng, L. Ying, F. Huang, Y. Cao, *Sci. China: Chem.* **2019**, *62*, 746.

[90] a) J. P. Correa-Baena, M. Saliba, T. Buonassisi, M. Gratzel, A. Abate, W. Tress, A. Hagfeldt, *Science* **2017**, *358*, 739; b) S. Shao, M. A. Loi, *Adv. Mater. Interfaces* **2019**, *7*, 1901469.

[91] K. A. Mazzio, C. K. Luscombe, *Chem. Soc. Rev.* **2015**, *44*, 78.

[92] L. Lu, T. Zheng, Q. Wu, A. M. Schneider, D. Zhao, L. Yu, *Chem. Rev.* **2015**, *115*, 12666.

[93] Y. C. Liu, C. S. Li, Z. J. Ren, S. K. Yan, M. R. Bryce, *Nat. Rev. Mater.* **2018**, *3*, 20.

[94] a) G. A. H. Wetzelaer, A. Najafi, R. J. P. Kist, M. Kuik, P. W. M. Blom, *Appl. Phys. Lett.* **2013**, *102*, 053301; b) N. B. Kotadiya, H. Lu, A. Mondal, Y. Ie, D. Andrienko, P. W. M. Blom, G. Wetzelaer, *Nat. Mater.* **2018**, *17*, 329; c) P. de Bruyn, A. H. P. van Rest, G. A. H. Wetzelaer, D. M. de Leeuw, P. W. M. Blom, *Phys. Rev. Lett.* **2013**, *111*, 5.

[95] S. De Wolf, J. Holovsky, S.-J. Moon, P. Löper, B. Niesen, M. Ledinsky, F.-J. Haug, J.-H. Yum, C. Ballif, *J. Phys. Chem. Lett.* **2014**, *5*, 1035.

[96] Z.-K. Tan, R. S. Moghaddam, M. L. Lai, P. Docampo, R. Higler, F. Deschler, M. Price, A. Sadhanala, L. M. Pazos, D. Credgington, F. Hanusch, T. Bein, H. J. Snaith, R. H. Friend, *Nat. Nanotechnol.* **2014**, *9*, 687.

[97] J. Woo Choi, H. C. Woo, X. Huang, W.-G. Jung, B.-J. Kim, S.-W. Jeon, S.-Y. Yim, J.-S. Lee, C.-L. Lee, *Nanoscale* **2018**, *10*, 13356.

[98] T. Leijtens, S. D. Stranks, G. E. Eperon, R. Lindblad, E. M. J. Johansson, I. J. McPherson, H. Rensmo, J. M. Ball, M. M. Lee, H. J. Snaith, *ACS Nano* **2014**, *8*, 7147.

[99] W. Xu, Q. Hu, S. Bai, C. Bao, Y. Miao, Z. Yuan, T. Borzda, A. J. Barker, E. Tyukalova, Z. Hu, M. Kawecki, H. Wang, Z. Yan, X. Liu, X. Shi, K. Uvdal, M. Fahlman, W. Zhang, M. Duchamp, J.-M. Liu, A. Petrozza, J. Wang, L.-M. Liu, W. Huang, F. Gao, *Nat. Photonics* **2019**, *13*, 418.

[100] S. Reineke, M. Thomschke, B. Lüssem, K. Leo, *Rev. Mod. Phys.* **2013**, *85*, 1245.

[101] M. J. Alam, D. C. Cameron, *Thin Solid Films* **2000**, *377–378*, 455.

[102] D. S. Hecht, L. B. Hu, G. Irvin, *Adv. Mater.* **2011**, *23*, 1482.

**ADVANCED
SCIENCE NEWS**

www.advancedsciencenews.com

**ADVANCED
MATERIALS
TECHNOLOGIES**

www.advmattechnol.de

[103] J. Wu, H. A. Becerril, Z. Bao, Z. Liu, Y. Chen, P. Peumans, *Appl. Phys. Lett.* **2008**, *92*, 263302.

[104] Z. Yin, S. Sun, T. Salim, S. Wu, X. Huang, Q. He, Y. M. Lam, H. Zhang, *ACS Nano* **2010**, *4*, 5263.

[105] D. Konios, C. Petridis, G. Kakavelakis, M. Sygletou, K. Savva, E. Stratakis, E. Kymakis, *Adv. Funct. Mater.* **2015**, *25*, 2213.

[106] K. Sakamoto, H. Kuwae, N. Kobayashi, A. Nobori, S. Shoji, J. Mizuno, *Sci. Rep.* **2018**, *8*, 2825.

[107] Y.-X. Wang, S.-L. Chou, H.-K. Liu, S.-X. Dou, *Carbon* **2013**, *57*, 202.

[108] a) J. Krantz, M. Richter, S. Spallek, E. Spiecker, C. J. Brabec, *Adv. Funct. Mater.* **2011**, *21*, 4784; b) B. Sciacca, J. van de Groep, A. Polman, E. C. Garnett, *Adv. Mater.* **2016**, *28*, 905.

[109] S. Han, S. Hong, J. Ham, J. Yeo, J. Lee, B. Kang, P. Lee, J. Kwon, S. S. Lee, M. Y. Yang, S. H. Ko, *Adv. Mater.* **2014**, *26*, 5808.

[110] W. W. Xiong, H. L. Liu, Y. Z. Chen, M. L. Zheng, Y. Y. Zhao, X. B. Kong, Y. Wang, X. Q. Zhang, X. Y. Kong, P. F. Wang, L. Jiang, *Adv. Mater.* **2016**, *28*, 7167.

[111] J. Liang, L. Li, K. Tong, Z. Ren, W. Hu, X. Niu, Y. Chen, Q. Pei, *ACS Nano* **2014**, *8*, 1590.

[112] A. G. Ricciardulli, S. Yang, G. Wetzelaer, X. L. Feng, P. W. M. Blom, *Adv. Funct. Mater.* **2018**, *28*, 1706010.

[113] Y. Xu, G. Long, L. Huang, Y. Huang, X. Wan, Y. Ma, Y. Chen, *Carbon* **2010**, *48*, 3308.

[114] J. Geng, L. Liu, S. B. Yang, S.-C. Youn, D. W. Kim, J.-S. Lee, J.-K. Choi, H.-T. Jung, *J. Phys. Chem. C* **2010**, *114*, 14433.

[115] E. Kymakis, K. Savva, M. M. Stylianakis, C. Fotakis, E. Stratakis, *Adv. Funct. Mater.* **2013**, *23*, 2742.

[116] A. G. Ricciardulli, S. Yang, X. Feng, P. W. M. Blom, *ACS Appl. Mater. Interfaces* **2017**, *9*, 25412.

[117] M. Batmunkh, C. J. Shearer, M. J. Biggs, J. G. Shapter, *J. Mater. Chem. A* **2016**, *4*, 2605.

[118] J. Wu, M. Agrawal, H. A. Becerril, Z. Bao, Z. Liu, Y. Chen, P. Peumans, *ACS Nano* **2010**, *4*, 43.

[119] a) K. X. Steirer, J. P. Chesin, N. E. Widjonarko, J. J. Berry, A. Miedaner, D. S. Ginley, D. C. Olson, *Org. Electron.* **2010**, *11*, 1414; b) T. M. Brown, J. S. Kim, R. H. Friend, F. Cacialli, R. Daik, W. J. Feast, *Appl. Phys. Lett.* **1999**, *75*, 1679.

[120] S. Shao, J. Liu, J. Bergqvist, S. Shi, C. Veit, U. Würfel, Z. Xie, F. Zhang, *Adv. Energy Mater.* **2013**, *3*, 349.

[121] M. B. Islam, M. Yanagida, Y. Shirai, Y. Nabetani, K. Miyano, *ACS Omega* **2017**, *2*, 2291.

[122] Y. Shi, K. K. Kim, A. Reina, M. Hofmann, L.-J. Li, J. Kong, *ACS Nano* **2010**, *4*, 2689.

[123] S.-S. Li, K.-H. Tu, C.-C. Lin, C.-W. Chen, M. Chhowalla, *ACS Nano* **2010**, *4*, 3169.

[124] J. Liu, Y. Xue, L. Dai, *J. Phys. Chem. Lett.* **2012**, *3*, 1928.

[125] J.-S. Yeo, J.-M. Yun, Y.-S. Jung, D.-Y. Kim, Y.-J. Noh, S.-S. Kim, S.-I. Na, *J. Mater. Chem. A* **2014**, *2*, 292.

[126] Z. Wu, S. Bai, J. Xiang, Z. Yuan, Y. Yang, W. Cui, X. Gao, Z. Liu, Y. Jin, B. Sun, *Nanoscale* **2014**, *6*, 10505.

[127] J.-S. Yeo, R. Kang, S. Lee, Y.-J. Jeon, N. Myoung, C.-L. Lee, D.-Y. Kim, J.-M. Yun, Y.-H. Seo, S.-S. Kim, S.-I. Na, *Nano Energy* **2015**, *12*, 96.

[128] H. Li, L. Tao, F. Huang, Q. Sun, X. Zhao, J. Han, Y. Shen, M. Wang, *ACS Appl. Mater. Interfaces* **2017**, *9*, 38967.

[129] B. R. Lee, J.-W. Kim, D. Kang, D. W. Lee, S.-J. Ko, H. J. Lee, C.-L. Lee, J. Y. Kim, H. S. Shin, M. H. Song, *ACS Nano* **2012**, *6*, 2984.

[130] Y. Yang, X. Yang, W. Yang, S. Li, J. Xu, Y. Jiang, *Nanoscale Res. Lett.* **2014**, *9*, 537.

[131] X. Li, W. Zhang, Y. Wu, C. Min, J. Fang, *ACS Appl. Mater. Interfaces* **2013**, *5*, 8823.

[132] Q. Van Le, T. P. Nguyen, H. W. Jang, S. Y. Kim, *Phys. Chem. Chem. Phys.* **2014**, *16*, 13123.

[133] Y. Lin, B. Adilbekova, Y. Firdaus, E. Yengel, H. Faber, M. Sajjad, X. Zheng, E. Yarali, A. Seitkhan, O. M. Bakr, A. El-Labban, U. Schwingenschlögl, V. Tung, I. McCulloch, F. Laquai, T. D. Anthopoulos, *Adv. Mater.* **2019**, *31*, 1902965.

[134] a) R. Dai, Y. Wang, J. Wang, X. Deng, *ChemSusChem* **2017**, *10*, 2869; b) A. Capasso, F. Matteocci, L. Najafi, M. Prato, J. Buha, L. Cinà, V. Pellegrini, A. D. Carlo, F. Bonaccorso, *Adv. Energy Mater.* **2016**, *6*, 1600920.

[135] a) M. Park, T. P. Nguyen, K. S. Choi, J. Park, A. Ozturk, S. Y. Kim, *Electron. Mater. Lett.* **2017**, *13*, 344; b) C.-W. Liu, C. Wang, C.-W. Liao, J. Golder, M.-C. Tsai, H.-T. Young, C.-T. Chen, C.-I. Wu, *AIP Adv.* **2018**, *8*, 045006.

[136] W. Chen, K. Li, Y. Wang, X. Feng, Z. Liao, Q. Su, X. Lin, Z. He, *J. Phys. Chem. Lett.* **2017**, *8*, 591.

[137] M. Batmunkh, M. Bat-Erdene, J. G. Shapter, *Adv. Energy Mater.* **2018**, *8*, 1701832.

[138] A. G. Ricciardulli, S. Yang, N. B. Kotadiya, G.-J. A. H. Wetzelaer, X. Feng, P. W. M. Blom, *Adv. Electron. Mater.* **2019**, *5*, 1800687.

[139] J.-M. Yun, J.-S. Yeo, J. Kim, H.-G. Jeong, D.-Y. Kim, Y.-J. Noh, S.-S. Kim, B.-C. Ku, S.-I. Na, *Adv. Mater.* **2011**, *23*, 4923.

[140] C. T. G. Smith, R. W. Rhodes, M. J. Beliatis, K. D. G. I. Jayawardena, L. J. Rozanski, C. A. Mills, S. R. P. Silva, *Appl. Phys. Lett.* **2014**, *105*, 073304.

[141] I. P. Murray, S. J. Lou, L. J. Cote, S. Loser, C. J. Kadleck, T. Xu, J. M. Szarko, B. S. Rolczynski, J. E. Johns, J. Huang, L. Yu, L. X. Chen, T. J. Marks, M. C. Hersam, *J. Phys. Chem. Lett.* **2011**, *2*, 3006.

[142] X. Yang, W. Fu, W. Liu, J. Hong, Y. Cai, C. Jin, M. Xu, H. Wang, D. Yang, H. Chen, *J. Mater. Chem. A* **2014**, *2*, 7727.

[143] K. Yan, Z. Wei, J. Li, H. Chen, Y. Yi, X. Zheng, X. Long, Z. Wang, J. Wang, J. Xu, S. Yang, *Small* **2015**, *11*, 2269.

[144] Y. G. Kim, K. C. Kwon, Q. V. Le, K. Hong, H. W. Jang, S. Y. Kim, *J. Power Sources* **2016**, *319*, 1.

[145] S. Shi, V. Sadhu, R. Moubah, G. Schmerber, Q. Bao, S. R. P. Silva, *J. Mater. Chem. C* **2013**, *1*, 1708.

[146] a) W. Zhu, M. N. Yogeesh, S. Yang, S. H. Aldave, J.-S. Kim, S. Sonde, L. Tao, N. Lu, D. Akinwande, *Nano Lett.* **2015**, *15*, 1883; b) Y. Zhang, J. Ye, Y. Matsuhashi, Y. Iwasa, *Nano Lett.* **2012**, *12*, 1136.

[147] X. Bao, Q. Ou, Z.-Q. Xu, Y. Zhang, Q. Bao, H. Zhang, *Adv. Mater. Technol.* **2018**, *3*, 1800072.

[148] J. T.-W. Wang, J. M. Ball, E. M. Barea, A. Abate, J. A. Alexander-Webber, J. Huang, M. Saliba, I. Mora-Sero, J. Bisquert, H. J. Snaith, R. J. Nicholas, *Nano Lett.* **2014**, *14*, 724.

[149] Z. Zhu, J. Ma, Z. Wang, C. Mu, Z. Fan, L. Du, Y. Bai, L. Fan, H. Yan, D. L. Phillips, S. Yang, *J. Am. Chem. Soc.* **2014**, *136*, 3760.

[150] Q. Van Le, T. P. Nguyen, K. S. Choi, Y.-H. Cho, Y. J. Hong, S. Y. Kim, *Phys. Chem. Chem. Phys.* **2014**, *16*, 25468.

[151] a) W.-Y. Tan, R. Wang, M. Li, G. Liu, P. Chen, X.-C. Li, S.-M. Lu, H. L. Zhu, Q.-M. Peng, X.-H. Zhu, W. Chen, W. C. H. Choy, F. Li, J. Peng, Y. Cao, *Adv. Funct. Mater.* **2014**, *24*, 6540; b) H. Zhang, W.-Y. Tan, S. Fladischer, L. Ke, T. Ameri, N. Li, M. Turbiez, E. Spiecker, X.-H. Zhu, Y. Cao, C. J. Brabec, *J. Mater. Chem. A* **2016**, *4*, 5032; c) N. Chakravarthi, K. Gunasekar, W. Cho, D. X. Long, Y.-H. Kim, C. E. Song, J.-C. Lee, A. Facchetti, M. Song, Y.-Y. Noh, S.-H. Jin, *Energy Environ. Sci.* **2016**, *9*, 2595.

[152] S. Lin, S. Liu, Z. Yang, Y. Li, T. W. Ng, Z. Xu, Q. Bao, J. Hao, C.-S. Lee, C. Surya, F. Yan, S. P. Lau, *Adv. Funct. Mater.* **2016**, *26*, 864.

[153] M. A. Ibrahem, T.-W. Lan, J. K. Huang, Y.-Y. Chen, K.-H. Wei, L.-J. Li, C. W. Chu, *RSC Adv.* **2013**, *3*, 13193.